Structural basis for template switching by a group II intron–encoded non-LTR-retroelement reverse transcriptase

Received for publication, May 15, 2021, and in revised form, June 30, 2021 Published, Papers in Press, July 17, 2021,
https://doi.org/10.1016/j.jbc.2021.100971

Alfred M. Lentzsch, Jennifer L. Stamos, Jun Yao, Rick Russell, and Alan M. Lambowitz*
From the Departments of Molecular Biosciences and Oncology, University of Texas at Austin, Austin, Texas, USA

Edited by Karin Musier-Forsyth

Reverse transcriptases (RTs) can switch template strands during complementary DNA synthesis, enabling them to join discontinuous nucleic acid sequences. Template switching (TS) plays crucial roles in retroviral replication and recombination, is used for adapter addition in RNA-Seq, and may contribute to retroelement fitness by increasing evolutionary diversity and enabling continuous complementary DNA synthesis on damaged templates. Here, we determined an X-ray crystal structure of a TS complex of a group II intron RT bound simultaneously to an acceptor RNA and donor RNA template–DNA primer heteroduplex with a 1-nt 3′-DNA overhang. The structure showed that the 3′ end of the acceptor RNA binds in a pocket formed by an N-terminal extension present in non–long terminal repeat–retroelement RTs and the RT fingertips loop, with the 3′ nucleotide of the acceptor base paired to the 1-nt 3′-DNA overhang and its penultimate nucleotide base paired to the incoming dNTP at the RT active site. Analysis of structure-guided mutations identified amino acids that contribute to acceptor RNA binding and a phenylalanine residue near the RT active site that mediates nontemplated nucleotide addition. Mutation of the latter residue decreased multiple sequential template switches in RNA-Seq. Our results provide new insights into the mechanisms of TS and nontemplated nucleotide addition by RTs, suggest how these reactions could be improved for RNA-Seq, and reveal common structural features for TS by non–long terminal repeat–retroelement RTs and viral RNA–dependent RNA polymerases.

Reverse transcriptases (RTs) are a large enzyme family, members of which function in the replication of human pathogens, such as retroviruses and hepatitis B virus, have played pivotal roles in the evolution of life on earth, and are widely used for biotechnological applications, such as RT-PCR and RNA-Seq (1–4). Although most studies have focused on retroviral enzymes and other RTs found in eukaryotes, RTs are thought to have originated in bacteria, likely from an RNA-dependent RNA polymerase (RdRP), and large numbers of RTs persist there, either encoded by retrotransposons called mobile group II introns or as free-standing genomically encoded enzymes (5–9). The latter are related to group II intron RTs but have acquired cellular functions, including phage/host tropism switching, acquisition of RNA spacers in CRISPR–Cas systems, and contributions to multiple types of phage defense mechanisms (10–13). These bacterial enzymes provide an evolutionary perspective on the biochemical properties and biological functions of RTs, which are much wider than suggested by a narrow focus on retroviral RTs.

Template switching (TS) is an important but as yet poorly understood biochemical activity of RTs and RdRPs. Studies of TS by retroviral RTs focused initially on its role in retroviral replication and recombination and more recently on its use for adapter addition in RNA-Seq (1, 14–16). TS by retroviral RTs is dependent upon base pairing between the donor and acceptor nucleic acids and falls into two mechanistically distinct categories: strand transfers, which require long base-pairing interactions between the donor and acceptor nucleic acids, such as those involving long terminal repeat (LTR) sequences during retroviral replication, and end-to-end clamping, which typically requires only two to four base pairs and is dependent upon nontemplated nucleotide addition (NTA) to a completed complementary DNA (cDNA) (17–20). Retroviral RT clamping is employed in a widely used high-throughput RNA-Seq method called SMART-Seq for 5′ RNA-Seq adapter addition by TS from the 5′ end of an RNA template to a synthetic adapter oligonucleotide whose 3′ end contains nucleotide residues complementary to those added by NTA to the 3′ end of a completed cDNA (14–16).

Group II intron and other bacterial RTs belong to a large subgroup of RTs that are encoded by non-LTR-retroelements and includes mitochondrial retroplasmid, human LINE-1 element, insect R2 element, and other eukaryotic non-LTR-retrotransposon RTs (2, 21). Non-LTR-retroelement RTs are homologous to retroviral RTs but have distinctive structural features, including a functionally important N-terminal extension (NTE) and two insertions, denoted RT2a and RT3a, between conserved sequence blocks in the fingers and palm of the RT domain (21, 22). An X-ray crystal structure of a full-length group II intron RT (the thermostable *Geobacillus stearothermophilus* GsI-IIC RT, sold commercially as thermostable group II intron reverse transcriptase III [TGIRT-III]) bound to template–primer substrate, and an incoming dNTP showed that these insertions contribute multiple additional contacts with RNA templates and more constrained binding

* For correspondence: Alan M. Lambowitz, lambowitz@austin.utexas.edu.
Present address for Alfred M. Lentzsch: Division of Chemistry and Chemical Engineering, California Institute of Technology, Pasadena, CA, USA.

sites for the templating RNA base, 3′ end of the DNA primer, and incoming dNTP that could contribute to the relatively high fidelity and processivity of group II intron RTs (23, 24). Structural cognates of all three of these distinctive regions are also found in RdRPs but are not present and presumed to have been lost from retroviral RTs, which evolved to evade host defenses by introducing frequent mutational variations and rapidly propagating beneficial ones by falling off one template and using the bound cDNA as a primer to reinitiate on another (24–26).

Studies in our laboratory aided by the crystal structure described previously have focused on the TS activity of GsI-IIC RT (27). In a previous biochemical study, we used a series of synthetic acceptor RNAs and donor RNA template–DNA heteroduplexes representing the 5′ end of an RNA template annealed to a completed cDNA to establish a kinetic framework for the TS and related NTA reactions of this enzyme (27). These studies showed that TS is most efficient from a donor RNA–DNA heteroduplex with a 1-nt 3′-DNA overhang complementary to the 3′ nucleotide of the acceptor RNA, indicating a requirement for a single NTA to the 3′ end of the completed cDNA, and that the single base pair between the 1-nt 3′-DNA overhang and the 3′ nucleotide of the acceptor confers remarkably high specificity (97.5–99.7% precise junctions depending upon the base pair), as determined by high-throughput sequencing of the TS junctions (27).

Here, we determined a crystal structure of GsI-IIC RT in the act of TS, to our knowledge the first such structure for any polymerase. The structure showed that the 3′ end of the acceptor RNA template binds in a pocket that is formed by the NTE and fingertips loop and is ordinarily occupied by upstream regions of a continuous RNA template. The structure provides new mechanistic insights, including how a single initial base-pairing interaction within the TS pocket could lead to highly specific TS junctions, and suggests how the TS and NTA reactions might be improved for RNA-Seq applications. A similar TS pocket composed of a homologous NTE and fingertips loop is conserved in non-LTR-retroelement RTs and viral RdRPs, but only partially conserved in retroviral RTs, which lack the NTE and exhibit more promiscuous TS behavior.

Results

Structure of a group II intron RT TS complex

We determined a crystal structure of full-length *Escherichia coli*–expressed GsI-IIC RT in complex with a 5-nt acceptor RNA (5′ rUrUrUrUrG), a donor duplex consisting of a 10-nt RNA template strand annealed to a complementary 11-nt DNA primer strand leaving a 1-nt 3′ dideoxy C overhang, and dATP (Fig. 1, *A* and *B* and Table S1). The donor duplex represents the 5′ end of an RNA template annealed to a completed cDNA after NTA of a nucleotide complementary to the 3′ nucleotide of the acceptor RNA but unable to initiate cDNA synthesis because of the 3′ dideoxy. Nucleotide residues in the structure are designated as belonging to the primer (P) or template (T) strands and are numbered positively or negatively from the dNTP-binding site at position −1, with T-1 (a U residue) corresponding to the templating RNA base for the incoming dATP (Fig. 1*B*).

The complex crystallized in the space group C2, with the asymmetric unit containing two pseudosymmetric RT monomers, each bound to the acceptor RNA and donor duplex. We determined initial phases by molecular replacement, using the previously determined GsI-IIC RT structure as the search model (Protein Data Bank [PDB] ID: 6AR3; (24)) with the dATP and parts of the template strand removed to reduce model bias. Similar to the previously solved GsI-IIC RT structure, we encountered problems of crystal twinning, discussed in detail in the prior work (24). Calculated composite omit maps showed reasonable backbone density near the active site, acceptor RNA, and donor duplex (Fig. S1), but amino acid side-chain density for some residues was not well defined, likely because of a combination of low resolution and more severe crystal twinning than for the previous GsI-IIC RT structure with a continuous RNA template (PDB ID: 6AR1). Based on the similarity between the two structures, poorly defined side-chain positions in regions outside the donor–acceptor junction in the TS structure were assumed to be similar to those in the previous continuous-template structure, and key features of the structure were confirmed biochemically. We were able to refine the structure to R_{Work} and R_{Free} values of 27.1% and 32.4% at 3.2-Å resolution with other collection and refinement statistics summarized in Table 1. We were unable to crystallize the complex in the absence of dATP or with donor duplexes having a blunt end or mismatched 3′-overhang nucleotide. These findings suggest that both base pairing of the 3′ nucleotide of the acceptor to the 1-nt 3′-overhang nucleotide of the DNA oligonucleotide and binding of a dNTP complementary to the templating RNA base are required for the RT to form a crystallizable complex.

The overall conformation of GsI-IIC RT in the TS complex was largely the same as that bound to a continuous RNA template (PDB ID: 6AR1 (24)) (Fig. 1*A*). The protein follows the canonical hand-like fold of other RTs with fingers, palm, and thumb regions, plus an appended DNA-binding domain (D) that contributes to DNA target site recognition during group II intron mobility ("retrohoming") to a new DNA site (Fig. 1*A*) (2). The last three nucleotides of the acceptor RNA (T+1 to T-2) sit within a pocket that is formed by the NTE and the fingertips loop and would ordinarily be occupied by upstream regions of a continuous RNA template (Fig. 2). T-3, which lies outside the TS pocket, is ordered as a result of a crystal contact to a symmetry-related GsI-IIC RT thumb domain, whereas the 5′ nucleotide of the acceptor (T-4), which lies farther outside the TS pocket, could not be modeled and is likely disordered.

In agreement with the TS mechanism inferred from biochemical analysis (27), the 3′ G of the acceptor RNA at T+1 is base paired to the 3′-overhang nucleotide of the DNA primer (P+1) at the position corresponding to a newly formed base pair after translocation out of the RT active site, whereas the

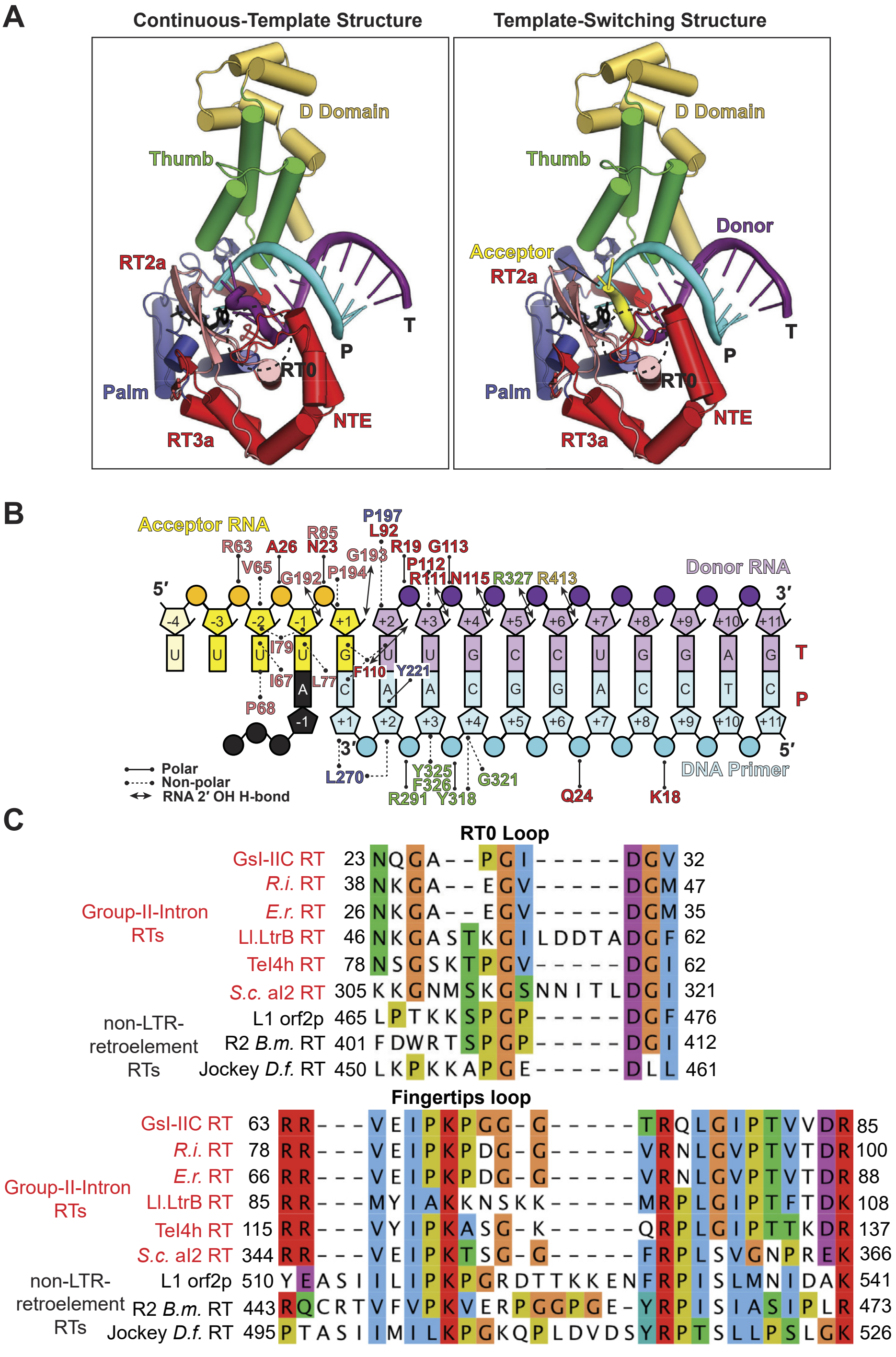
A
Continuous-Template Structure
Template-Switching Structure
D Domain
Thumb
RT2a
Palm
RT0
P
T
NTE
RT3a
Acceptor
Donor
B
Acceptor RNA
Donor RNA
5′
3′
-4 -3 -2 -1 +1 +2 +3 +4 +5 +6 +7 +8 +9 +10 +11
U U U U G U U G C C U G G A G
A C A A C G G A C C T C
T
P
R63 A26 N23 R85 G193 P197 L92 R19 G113
V65 G192 P194 P112 R111 N115 R327 R413
I79 I67 L77 F110 Y221 P68
L270 Y325 F326 R291 Y318 G321 Q24 K18
DNA Primer
Polar
Non-polar
RNA 2′ OH H-bond
C
RT0 Loop
Group-II-Intron RTs
GsI-IIC RT 23 NQGA--PGI-----DGV 32
R.i. RT 38 NKGA--EGV-----DGM 47
E.r. RT 26 NKGA--EGV-----DGM 35
Ll.LtrB RT 46 NKGASTKGILDDTADGF 62
Tel4h RT 78 NSGSKTPGV-----DGI 62
S.c. al2 RT 305 KKGNMSKGSNNITLDGI 321
non-LTR-retroelement RTs
L1 orf2p 465 LPTKKSPGP-----DGF 476
R2 B.m. RT 401 FDWRTSPGP-----DGI 412
Jockey D.f. RT 450 LKPKKAPGE-----DLL 461
Fingertips loop
GsI-IIC RT 63 RR---VEIPKPGG-G-----TRQLGIPTVVDR 85
R.i. RT 78 RR---VEIPKPDG-G-----VRNLGVPTVTDR 100
E.r. RT 66 RR---VEIPKPDG-G-----VRNLGVPTVTDR 88
Ll.LtrB RT 85 RR---MYIAKKNSKK-----MRPLGIPTFTDK 108
Tel4h RT 115 RR---VYIPKASG-K------QRPLGIPTTKDR 137
S.c. al2 RT 344 RR---VEIPKTSG-G-----FRPLSVGNPREK 366
L1 orf2p 510 YEASIILIPKPGRDTTKKENFRPISLMNIDAK 541
R2 B.m. RT 443 RQCRTVFVPKVERPGGPGE-YRPISIASIPLR 473
Jockey D.f. RT 495 PTASIIMILKPGKQPLDVDSYRPTSLLPSLGK 526

Figure 1. Structure of a group II intron RT template-switching (TS) complex. *A*, structure of GsI-IIC RT poised for TS from a donor RNA template–DNA primer heteroduplex to an acceptor RNA template (*right*) compared with that of GsI-IIC RT bound to a continuous RNA template–DNA primer heteroduplex (*left*; Protein Data Bank ID: 6AR1). Protein regions: fingers (*salmon*), insertions (*red*), palm (*dark blue*), thumb (*green*), D domain (*gold*), acceptor RNA template (*yellow*), donor RNA template (*purple*), DNA primer (*cyan*), and dATP (*black*). T and P denote the template and primer strands, respectively. The RT0 loop is highlighted in a *dotted circle*. *B*, schematic of protein–nucleic acid interactions in the TS structure. Nucleotide positions are denoted as template (T) or primer (P) strand numbered from the templating nucleotide at the RT active site (T-1). Interactions between nucleic acid and amino acid residues are indicated by a *black line* (polar interaction), *dotted line* (nonpolar interaction), or a *double-headed arrow* (RNA 2′ OH H-bond). Other color codes are as in panel *A*. The first nucleotide of the acceptor (the U at T-4) could not be modeled and is shown in a *lighter shade of yellow*. *C*, amino acid sequence alignments of the RT0 loop (*top*) and fingertips loop (*bottom*) regions of group II intron RTs (*red*; GsI-IIC RT [E2GM63], *Roseburia intestinalis* [D4L313], *Eubacterium rectale* [D4JMT6], Ll.LtrB [P0A3U0], Tel4h [Q8DMK2], *Saccharomyces cerevisiae* aI2 [P03876]) and non-LTR-retroelement RTs (*black*; human LINE-1 [LI], orf2p [O00370], R2 *Bombyx mori* [V9H052], and Jockey *Drosophila funebris* RT [P21329]). Uniprot IDs are indicated in parentheses. Protein sequences were aligned using the MAFFT algorithm and colored using ClustalX settings. RT, reverse transcriptase.

penultimate nucleotide of the acceptor at T-1 occupies the position of the templating base and is base paired to the incoming dATP at the RT active site (Fig. 1*A*). The high specificity of TS likely reflects that these two base-pairing interactions occur sequentially, with the second between the templating base and incoming dNTP accompanied by a conformational change

Table 1

Collection and refinement statistics for the GsI-IIC RT TS complex structure

Data collection	
Wavelength	0.9774 Å
Resolution range	48.3–3.2 (3.31–3.2)
Space group	C 1 2 1
Unit cell: a, b, c (Å); α, β, γ (°)	179.4, 107.4, 72.0; 90, 113.7, 90
Total reflections	141,238 (14,015)
Unique reflections	20,706 (2057)
Multiplicity	6.8 (6.8)
Completeness (%)	99.7 (99.9)
Mean I/sigma (I)	16.4 (2.49)
Wilson *B*-factor	85
R_{merge}	0.0775 (0.646)
R_{measure}	0.0841 (0.700)
R_{pim}	0.0323 (0.268)
CC1/2	0.999 (0.944)
CC*	1 (0.985)
Refinement	
Reflections used in refinement	20,704 (2057)
Reflections used for R_{Free}	2074 (237)
R_{Work}	0.271 (0.573)
R_{Free}	0.324 (0.590)
CC (work)	0.795 (−0.003)
CC (free)	0.621 (−0.109)
Number of nonhydrogen atoms	7991
Macromolecules	7914
Ligands	77
Protein residues	843
RMS (bonds)	0.013
RMS (angles)	1.55
Ramachandran favored (%)	98.6
Ramachandran allowed (%)	1.2
Ramachandran outliers (%)	0.2
Rotamer outliers (%)	0.6
Clash score	11.5
Average *B*-factor	124.4
Macromolecules	124.4
Ligands	123.2
Number of TLS groups	10

TLS, Translation/Libration/Screw.
Statistics for the highest-resolution shell are shown in parentheses.

required for the initiation of reverse transcription, which drives the reaction forward (see Discussion section).

Most of the contacts between GsI-IIC RT and the acceptor RNA and donor duplex are indistinguishable at this resolution from those for the RNA template and annealed DNA primer in the continuous template structure (Fig. 1*B*) (24). The 3′ end of the RNA acceptor at T+1, which is base paired to the 1-nt DNA overhang, and the templating base at T-1 rest near the fingers/palm junction on an inner surface of the protein formed by residues F110 and G192 in the PQG loop, G193, and P194, with hydrogen bonds from the backbone carbonyls of G192 and G193 to the 2′ OHs of T-1 and T+1, respectively (Fig. 1*B*).

Near the junction between the donor and acceptor RNAs, the RT0 loop of the NTE is in the same conformation as in the continuous RNA template structure (Fig. 2*A*; RMSD = 0.851 Å). The N-terminal portion of the loop from residues N23 to A26 (Fig. 1*C*) forms a lid over the phosphate backbone of T+1 and T-1, with hydrogen bonds from the side chain of N23 to the T+1 phosphate and from the backbone amide of A26 to the T-1 phosphate (Fig. 2*A*). As in other structures of group II intron RTs, including high-resolution crystal structures of N-terminal group II intron RT fragments without bound nucleic acids, the RT0 loop is well defined and anchored to the body of the protein by conserved hydrophobic residues at the central tip and C-terminal end of the loop (I29 and V32, respectively) and by hydrogen bonds between the side chain of R85 in the fingers and the backbone carbonyls of G25 and A26 in the loop (24, 28–30) (Figs. 1*B* and 2*C*). A highly conserved aspartate residue (D30) hydrogen bonds to the nearby G31 backbone amide (Fig. 2*C*). It may also form a hydrogen bond to T81 of the fingers, but this interaction is not conserved in other group II intron RT structures (28–30).

In the continuous template structure, N23 at the beginning of the RT0 loop rests midway between the two phosphate groups on either side of T+1, which corresponds to the 3′ nucleotide of the acceptor. In the TS structure, however, where T+1 is separated from the 5′ nucleotide of the donor (T+2) by a gap lacking a phosphate group, N23 shifts away from this position to suggest a closer interaction with the phosphate between T-1 and T+1, to which R85 from the fingers hydrogen bonds on the opposite side (Figs. 1*B* and 2, *A* and *B*). The adjacent residue, Q24, interacts with the phosphate of the primer strand between positions P+6 and P+7, potentially helping to anchor the donor duplex near the TS junction.

The remaining binding surface for the acceptor RNA within the TS pocket is provided by the fingertips loop, a conserved structural feature found in all RTs (Fig. 2, *B* and *C*). The fingertips loop consists of two antiparallel β strands, which are hinged and upon dNTP binding move the side chains of positively charged residues (R75 and K69 in GsI-IIC RT) into the RT active site to properly position the dNTP substrate and stabilize the negative charges of the triphosphate (31, 32). In the TS structure, the fingertips loop is closed over the RT active site in the same conformation as in the continuous template structure (RMSD = 0.684 Å; Fig. 2*C*). The opposite face of the fingertips loop contains a series of conserved branched hydrophobic residues that cradle the underside of the RNA acceptor at T-1 and T-2, with L77 and I79 contacting the T-1 base and ribose, respectively, and V65 and I67 contacting the T-2 ribose and base, respectively (Fig. 2, *B* and *C*; see also Fig. 5*A*). R63, which is located at the base of the fingertips loop, forms a polar contact to the phosphate connecting T-2 and T-3, representing the 5′-most interaction of the RT with the acceptor RNA in the TS pocket, whereas P68, which sits near the end of the fingertips loop between the two β strands, makes a distant nonpolar interaction with the base of T-2 (Figs. 1*B* and 2, *B* and *C*; see also Fig. 5*A*). The contacts between the six fingertips loop residues identified as binding the acceptor RNA were not detectably changed when compared with the continuous template structure (24). These six residues together with N23 of the NTE are often conserved in group II intron RTs (Fig. 1*C*) and potentially represent important contacts for TS.

TS of WT GsI-IIC RT and effect of mutations in the RT0 loop

To investigate the functions of the amino acid residues identified in the crystal structure as making side-chain contacts with the acceptor RNA, we constructed a series of GsI-

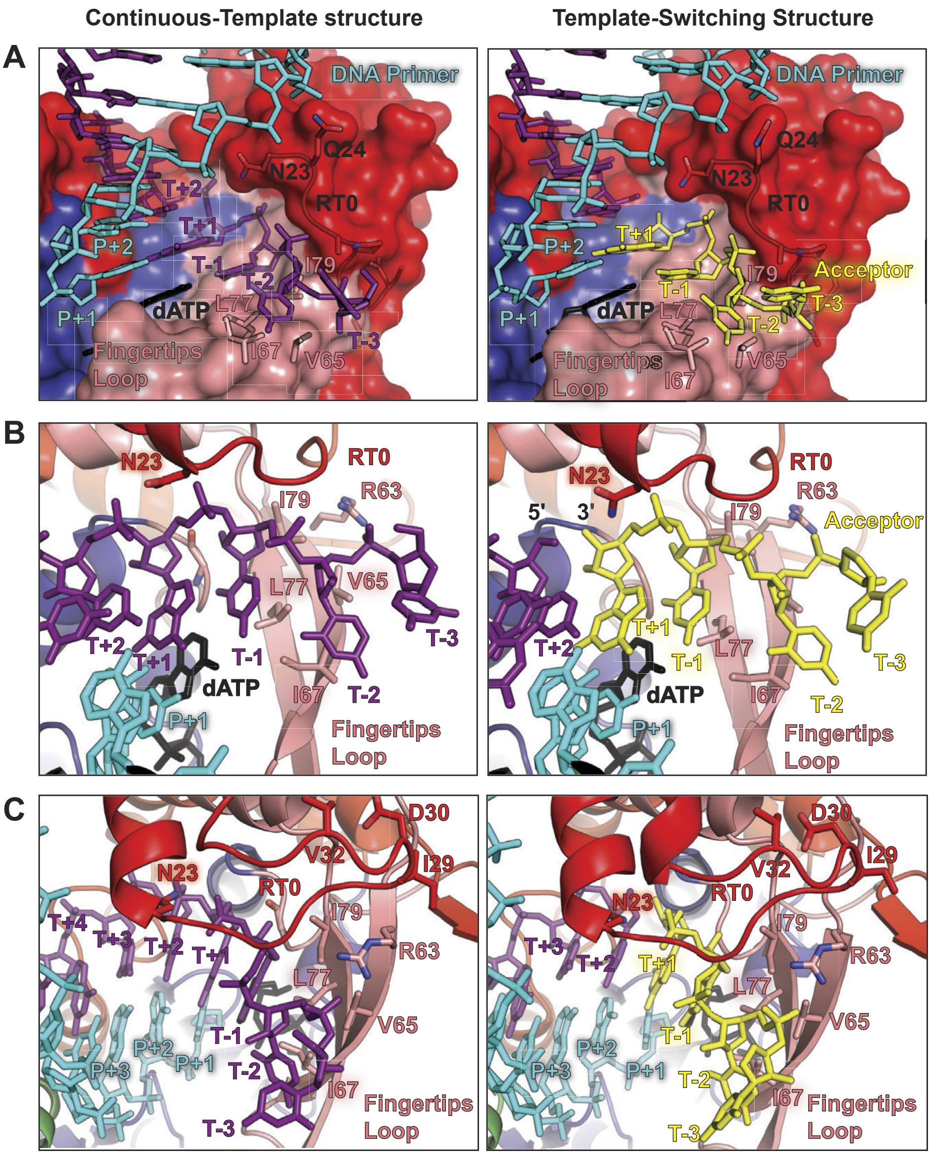

Figure 2. Binding of the 3′ end of the acceptor RNA within the template-switching (TS) pocket. *A*, close-up views comparing the binding of the 3′ end of the acceptor within the TS pocket formed by the NTE and fingertips loop (*right*) with the binding of a continuous RNA template in the same region of the protein (*left*; Protein Data Bank ID: 6AR1). Protein regions: fingers (*salmon*), insertions (*red*), palm (*dark blue*); acceptor RNA template (*yellow*), donor RNA or continuous template (*purple*), DNA primer (*cyan*), and dATP (*black*). Nucleic acids are depicted as *sticks*, and the protein is depicted in surface-filling representation with some residues highlighted as *sticks*. *B*, comparison of the same structures with rotation to give a better view of the junction region between the donor and acceptor RNA templates. Nucleic acids and protein regions are colored as in panel *A*. Nucleic acids are in stick representation, and protein is in cartoon representation with some residues highlighted as *sticks*. *C*, comparisons of the same structures with rotation to show the binding of the 3′ end of the acceptor beneath the "lid" of the RT0 loop within the TS pocket. Nucleic acids and protein regions are colored and shown in the same representation as in panel *B*. NTE, N-terminal extension.

IIC RT mutants and compared their TS and primer extension (PE) activities to those of the WT enzyme. Since we were interested in mutations that might affect binding of the acceptor, we first examined the TS activity of the WT enzyme as a function of acceptor RNA concentration (Fig. 3). To monitor binding of the acceptor and subsequent nucleotide incorporation, we used saturating dNTP concentrations with varying concentrations of a 21-nt acceptor RNA with a 3′-C residue and a fixed concentration of a donor RNA–DNA heteroduplex with a complementary 1-nt 3′-G DNA overhang (20 nM, substoichiometric relative to enzyme). Except for the fixed 1-nt 3′-G overhang, the donor duplex used for biochemical experiments corresponds to a version used for TGIRT-Seq and is unrelated to the shorter donor duplex used for crystallization (see the legend to Fig. 3 and Table S1).

The TS products in these experiments showed a characteristic ladder of bands that differ by 21 nt, reflecting multiple sequential template switches from the 5′ end of one RNA template to the 3′ end of another (Fig. 3*B*). Reaction time courses revealed a single predominant kinetic phase for the appearance of TS products, giving an observed rate constant (k_{obs}) for each acceptor RNA concentration (Fig. 3*B*). A fit of the observed rate constant as a function of acceptor concentration gave a maximal rate constant for TS (k_{TS}) of 0.23 ±

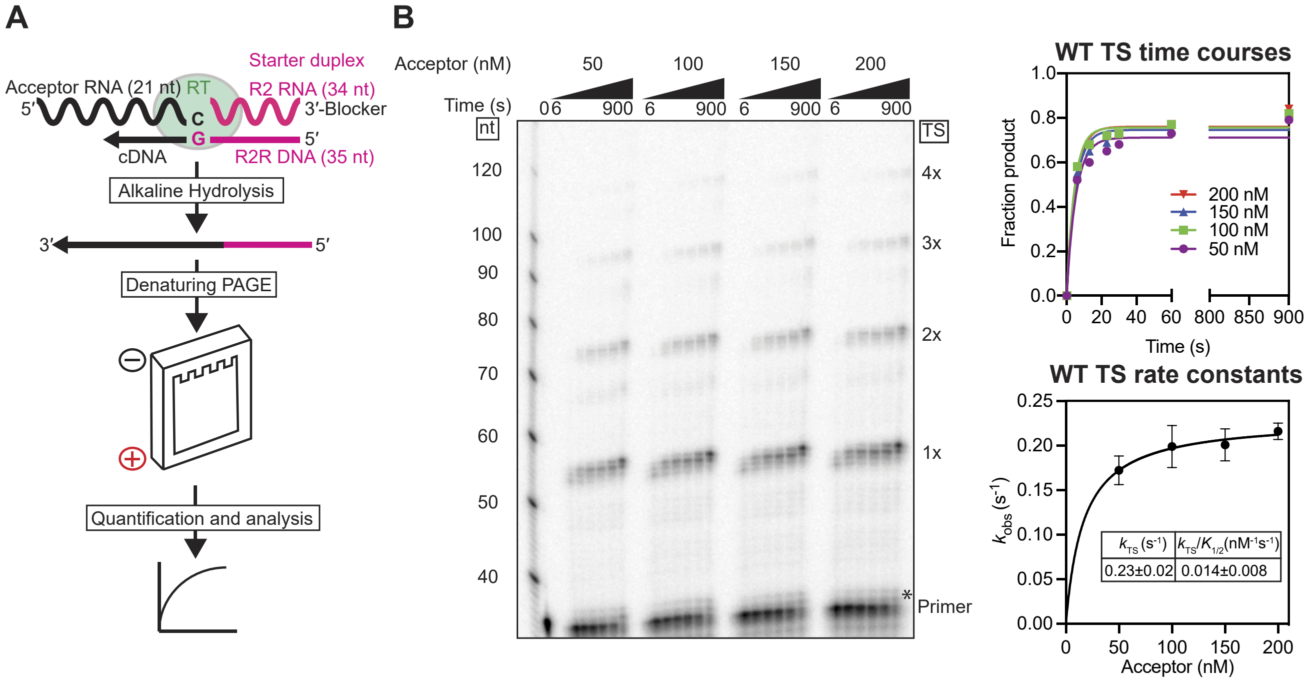

Figure 3. Overview of template-switching (TS) assays and determination of saturating acceptor RNA concentrations. *A*, outline of TS assay. GsI-IIC RT (*green oval*) was preincubated with a starter duplex (*magenta*) consisting of a 34-nt RNA oligonucleotide containing an Illumina Read 2 (R2) sequence annealed to a complementary 5′-^{32}P-labeled 35-nt DNA primer (R2R) leaving a 1-nt 3′-DNA overhang (nucleic acid sequences in Table S1). The 3′-DNA overhang nucleotide (G) base pairs with the 3′ nucleotide (C) of a 21-nt acceptor RNA (*black*) for TS, leading to the synthesis of a full-length complementary DNA of the acceptor RNA with the R2R oligonucleotide linked to its 5′ end. After incubation with NaOH to degrade RNA and neutralization with equimolar HCl, the complementary DNAs resulting from TS were analyzed by electrophoresis in a denaturing 6% polyacrylamide gel, which was dried and quantified with a phosphorimager. *B*, determination of saturating acceptor RNA concentrations. Time courses of TS reactions using 200 nM WT GsI-IIC RT and 20 nM donor RNA template–DNA primer duplex (5′-^{32}P-labeled on DNA primer) indicated concentrations of a 21-nt acceptor RNA template, and 4 mM dNTPs (an equimolar mix of 1 mM dATP, dCTP, dGTP, and dTTP) in reaction medium containing 200 mM NaCl at 60 °C. Aliquots were quenched at times ranging from 6 to 900 s, and the products were analyzed by denaturing PAGE. The figure shows a representative gel from one of three repeats of the experiment. The numbers to the left of the gel indicate size markers (a 5′-^{32}P-labeled single-stranded DNA ladder; ss20 DNA Ladder; Simplex Sciences) run in a parallel lane, and the labels to the right indicate products resulting from the initial template switch (1×) and subsequent end-to-end template switches from the 5′ end of one acceptor to the 3′ end of another (2×, 3×, etc.). The *asterisk* at the bottom right of the gel indicates the position of bands resulting from NTA to the 3′ end of the DNA primer. The plot at the *upper right* shows time courses of production of TS products (*i.e.*, products >2 nt larger than the primer) at each RNA acceptor concentration. The plot at the *bottom right* shows k_{obs} as a function of acceptor concentration fit by a hyperbolic equation to obtain the maximal rate constant k_{TS} and the second-order rate constant $k_{TS}/K_{1/2}$, with the error bars in the plot showing the standard error of the mean for three repeats of each time course and the uncertainties in the inset table indicating the standard error of the fit. RT, reverse transcriptase.

0.02 s^{-1}, in agreement with previous measurements done at saturating acceptor concentrations (0.25 s^{-1} (27)). The observed rate constant approached this maximum value even with the lowest concentration of acceptor (50 nM) that could be tested while maintaining the acceptor in excess of the GsI-IIC RT–starter duplex complex. Within this limited concentration-dependent regime, the fit gave an estimated second-order rate constant ($k_{TS}/K_{1/2}$) of 0.014 nM^{-1} s^{-1} ± 0.008. The latter value, also known as the specificity constant, represents the rate constant for acceptor binding multiplied by the probability of subsequent chain extension and was within two to three orders of magnitude of the diffusion limit, underscoring the efficiency of GsI-IIC RT for TS (Fig. 3*B*).

We previously compared the TS activities of WT and several mutant GsI-IIC RTs with alterations in conserved residues by using the same combination of a 3′-C acceptor RNA and 1-nt 3′-G DNA overhang donor duplex but in reactions incubated for a fixed time (15 min) at saturating concentrations of acceptor RNA and dNTPs (24). We found that mutations in a conserved anchoring residue in the RT0 loop (I29R; Fig. 1*C*) and in a conserved arginine in the fingers whose side chain hydrogen bonds to a backbone carbonyl in the RT0 loop and the phosphate between T-1 and T+1 of the acceptor (R85A; Fig. 1*C*) strongly inhibited TS while retaining high PE activity (24). By contrast, the mutation D30A, in another conserved residue that anchors the RT0 loop to the body of the protein, had no detectable effect on either TS or PE (24). In addition, the RT0 loop mutant 23-28/6G, in which the six residues at positions 23 to 28 were replaced by six glycines, retained high TS activity, whereas the mutant 23-31/4G, with a shorter RT0 loop in which residues 23 to 31 were replaced by four glycines, substantially inhibited TS activity (24). These findings suggested that the size and/or conformation of the RT0 loop might significantly impact TS.

Based on the aforementioned results and the crystal structure of the TS complex, we focused more detailed analysis on N23 and Q24, two solvent-exposed RT0 loop residues with prominent polar side-chain interactions with the acceptor backbone and donor duplex, respectively, and the RT0 loop mutant 23-31/4G, which inhibited TS activity in the previous assays (24). N23 was of interest as a conserved residue (Fig. 1*C*) whose side chain sits between the phosphates on either side of T+1 in the continuous-template structure but shifts closer to the upstream phosphate in the TS structure, where a downstream phosphate is not present in the gap between the donor and acceptor (Fig. 2*B*). This finding raised the possibilities that the N23 side chain could toggle between the two phosphates and that its interaction with the upstream phosphate could be particularly important for binding an acceptor RNA during TS, where there is a discontinuity in the phosphate backbone. The adjacent residue Q24 makes a side-chain polar contact with the phosphate between P+6 and P+7 on the primer strand, potentially anchoring the donor duplex near the TS junction (see previously mentioned one).

Nevertheless, we found that the mutants N23A, Q24G, N23A/Q24A, and N23G/Q24G had no effect on PE activity (Fig. S2) and displayed near-saturating kinetics at all the acceptor RNA concentrations tested, giving maximal rate constants of 0.28 to 0.32 s^{-1} and $k_{TS}/K_{1/2}$ values of ~0.01 to 0.02 nM^{-1} s^{-1}, indistinguishable from those of WT (Table 2 and Figs. 4 and S3). These results indicate that the side chains of N23 and Q24 do not play major roles in acceptor RNA binding or chain extension. It remains possible that Q24 stabilizes binding of the duplex, as the experiments were performed using a concentration of enzyme sufficient to saturate duplex binding.

The movement of the side chain of the N23 away from the gap between the donor and acceptor in the TS structure also led us to wonder whether adding a 5′ phosphate to the RNA donor would impact TS. To test this idea, we performed TS reactions with WT and N23A with the same acceptor RNA and either 5′ OH and 5′ phosphate donors (Fig. S4). For both proteins, TS activity with the 5′ phosphate donor decreased, likely because of steric clashes of the additional oxygen on the 5′ phosphate of donor compared with a phosphodiester bond (Fig. S4).

Finally, the mutation 23-31/4G had no detectable effect on PE activity (Fig. S2) but strongly inhibited TS activity, with the mutant showing subsaturating kinetics over the range of acceptor RNA concentrations tested with a decreased k_{TS} = 0.16 s^{-1} and a 3.5-fold lower $k_{TS}/K_{1/2}$ than the WT enzyme (Figs. 4 and S3 and Table 2) (24). These results indicate that the altered RT0 loop conformation, resulting from shortening of the loop and/or loss of the I29 anchoring interaction (see previously mentioned one), substantially inhibited binding of the acceptor RNA. The lack of effect of this mutation on PE indicates that when the TS pocket is occupied by a continuous RNA template the shorter glycine-rich RT0 loop is capable of adopting a conformation that does not impede reverse transcription.

TS of GsI-IIC RTs with mutations in the fingertips loop

The remaining residues that make potential critical side-chain contacts with the acceptor RNA are located in the fingertips loop, a conserved structural feature that forms part of the dNTP-binding pocket and contacts parts of the DNA primer and RNA acceptor. Here, we focused on five of the residues identified in the crystal structure as making side-chain contacts with acceptor RNA: R63, which is located at the base of the loop and makes a side-chain contact with the phosphate between T-2 and T-3; V65 and I67, which are located centrally in the first β-strand of the hairpin with their hydrophobic side chains engaged in nonpolar interactions with the ribose and base of T-2, respectively; and L77 and I79, which are located on the antiparallel β-strand with their side chains making nonpolar contacts with the sugar and base of T-1, the templating nucleotide at the RNA active site, and with the side chain of I79 also interacting with T-2 (Figs. 1 and 5). The mutation P68A is the sixth fingertips loop residue that makes a side-chain contact with the acceptor (a distant nonpolar contact paper with the base of T-2), did not inhibit TS in initial assays (Fig. S5*B*), and was not subjected to more detailed analysis.

To assess the contributions of the other fingertips loop residues to TS, we constructed the mutant R63A and double mutants V65A/I67A and L77A/I79A. The double mutant L77A/I79A had the strongest effect on TS, with a $k_{TS}/K_{1/2}$ value (0.0004 ± 0.0002 nM^{-1} s^{-1}; Figs. 5*B* and S5) that was 25-fold lower than that for WT (Fig. 3*B* and Table 2). R63A and V65A/I67A have k_{TS} values similar to WT but lower $k_{TS}/K_{1/2}$ values (0.0084 ± 0.01 and 0.0077 $nM^{-1}s^{-1}$ ± 0.005 compared with WT at 0.014 $nM^{-1}s^{-1}$; Table 2 and Figs. 3 and 5), most likely reflecting impaired binding of the acceptor RNA. All

Table 2
Summary of kinetic parameters determined for WT and mutant GsI-IIC RTs

Enzyme	Mutated region	k_{TS} (s^{-1})	$k_{TS}/K_{1/2}$ (nM^{-1} s^{-1})	$K_{1/2}$ (nM)	PE (nt/s)
WT	NA	0.23 ± 0.02	0.014 ± 0.008	~17	~20
N23A	RT0 loop	0.32 ± 0.07	0.0083 ± 0.005	~39	~20
Q24G	RT0 loop	0.30 ± 0.04	0.014 ± 0.01	~21	~20
N23A/Q24A	RT0 loop	0.32 ± 0.05	0.020 ± 0.018	~16	~20
N23G/Q24G	RT0 loop	0.28 ± 0.04	ND	ND	~20
23–31/4G	RT0 loop	0.16 ± 0.07	0.0037 ± 0.004	~44	~20
R63A	Fingertips loop	0.21 ± 0.06	0.0084 ± 0.01	~25	~20
V65A/I67A	Fingertips loop	0.25 ± 0.05	0.0077 ± 0.005	~33	~15
L77A/I79A	Fingertips loop	ND	0.00040 ± 0.0002	ND	~15
F143A	dNTP-binding site	0.19 ± 0.03	0.0034 ± 0.001	~56	~10

NA, not applicable; ND, not determined.
k_{TS} and $k_{TS}/K_{1/2}$ values are the best fit ± standard errors of the fit values obtained from fitting of a hyperbolic equation to the observed rate constants from two to three repeats of the time courses in the experiments of Figures 3–6 (see Experimental procedures section). $K_{1/2}$ values, which were not precisely determined by the time-course data because of saturation of the observed rate constants at low concentrations of acceptor for the WT and most of the mutants, are approximate values obtained from these fits, with relative uncertainties comparable to those for $k_{TS}/K_{1/2.}$ PE nt/s values are approximate mean values obtained from the midpoint of the 10 s time point in two to three repeats of the time courses in Figure S2.

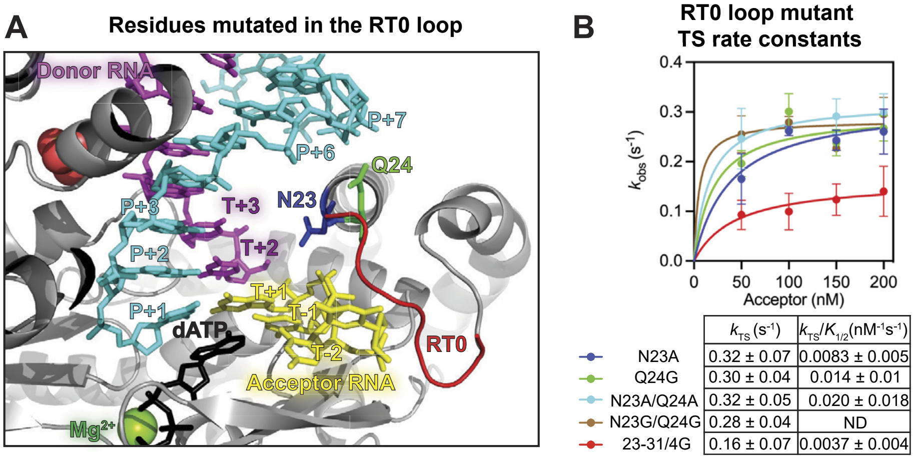

	k_{TS} (s^{-1})	$k_{TS}/K_{1/2}$($nM^{-1}s^{-1}$)
N23A	0.32 ± 0.07	0.0083 ± 0.005
Q24G	0.30 ± 0.04	0.014 ± 0.01
N23A/Q24A	0.32 ± 0.05	0.020 ± 0.018
N23G/Q24G	0.28 ± 0.04	ND
23-31/4G	0.16 ± 0.07	0.0037 ± 0.004

Figure 4. The effect of RT0 loop mutations on template switching by GsI-IIC RT. *A*, close-up view of the RT0 loop highlighting the location of mutated amino acid residues N23 (*blue stick*) and Q24 (*green stick*) and the polypeptide backbone of residues 23 to 31 (*red cartoon*). Nucleic acids are colored as in Figure 1, *A* and *B*. *B*, the plot shows k_{obs} as a function of acceptor concentration fit by a hyperbolic equation to obtain the maximal rate constant k_{TS} and the second-order rate constant $k_{TS}/K_{1/2}$. Template-switching reactions were done as described in Figure 3. Each rate constant measurement was performed twice, and representative time courses are shown in Figure S3. The error bars in the plot show the standard error of the mean, and the uncertainties in the k_{TS} and $k_{TS}/K_{1/2}$ values in the table below indicate the standard error of the fit. RT, reverse transcriptase

these mutants retained high PE activity (15–20 nt/s; Table 2 and Fig. S2), suggesting that the fingertips loop interactions are more critical for TS than for reverse transcription on a continuous RNA template.

Identification of an amino acid residue that is critical for NTA

Our previous kinetic analysis indicated that TS occurs largely by an ordered process in which a single nontemplated nucleotide is added to the 3′-end of a completed cDNA, thereby creating a 1-nt 3′-DNA overhang that can then base pair to the 3′ end of an acceptor RNA (27). To further investigate the contribution of NTA to TS, we focused on F143, which is located in the dNTP-binding pocket and may contribute to the selectivity of GsI-IIC RT for dNTPs by sterically blocking the 2′ OH present in rNTPs (24, 33). As in other RTs, the aromatic side chain of F143 is aligned for a pi-stacking interaction with the deoxyribose sugar of the incoming dNTP (Fig. 6*A*), and we hypothesized that this stabilizing interaction could be important for NTA, during which the added dNTP is not base paired with a templating nucleotide.

We constructed the mutant F143A and measured its kinetics of NTA to a blunt-end starter duplex in the absence of an acceptor RNA. We found that NTA was strongly diminished, with a ∼40-fold lower $k_{NTA}/K_{1/2}$ value than the WT enzyme (Figs. 6*B* and S6*A*). The decrease in rate was smaller at the highest dNTP concentrations measured, indicating that the decreased $k_{NTA}/K_{1/2}$ value is primarily because of weaker binding of the incoming dNTP (Figs. 6*B* and S6*A*). The F143A mutant retained substantial PE activity, synthesizing full-length cDNAs of a 1.1-kb RNA template with no indication

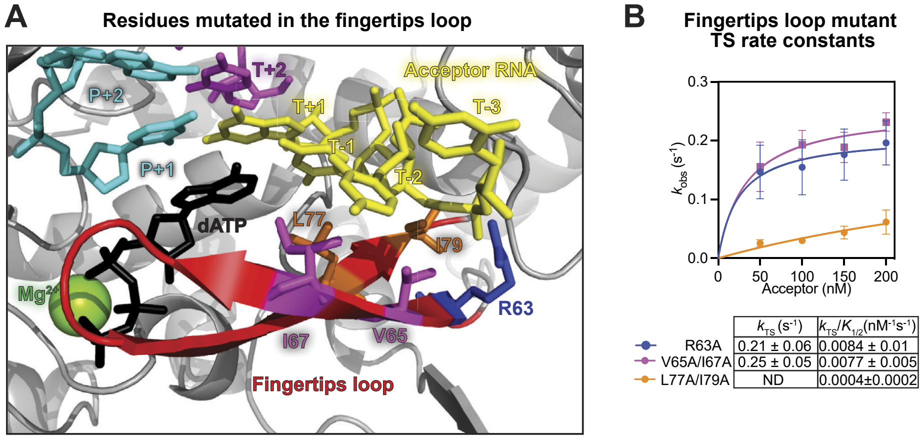

	k_{TS} (s^{-1})	$k_{TS}/K_{1/2}$($nM^{-1}s^{-1}$)
R63A	0.21 ± 0.06	0.0084 ± 0.01
V65A/I67A	0.25 ± 0.05	0.0077 ± 0.005
L77A/I79A	ND	0.0004±0.0002

Figure 5. The effect of fingertips loop mutations on template switching by GsI-IIC RT. *A*, close-up view of the fingertips loop (*red cartoon*) highlighting the location of mutated amino acid residues R63 (*blue stick*), V65/I67 (*magenta stick*), and L77/I79 (*orange stick*). Nucleic acids are colored as in Figure 1, *A* and *B*. *B*, the plot shows k_{obs} as a function of acceptor concentration fit by a hyperbolic equation to obtain the maximal rate constant k_{TS} and the second-order rate constant $k_{TS}/K_{1/2}$. Template-switching reactions were done as described in Figure 3, with each rate constant measurement performed twice and representative time courses shown in Figure S5. The error bars in the plot show the standard error of the mean, and the uncertainties in the k_{TS} and $k_{TS}/K_{1/2}$ values in the table below indicate the standard error of the fit. RT, reverse transcriptase.

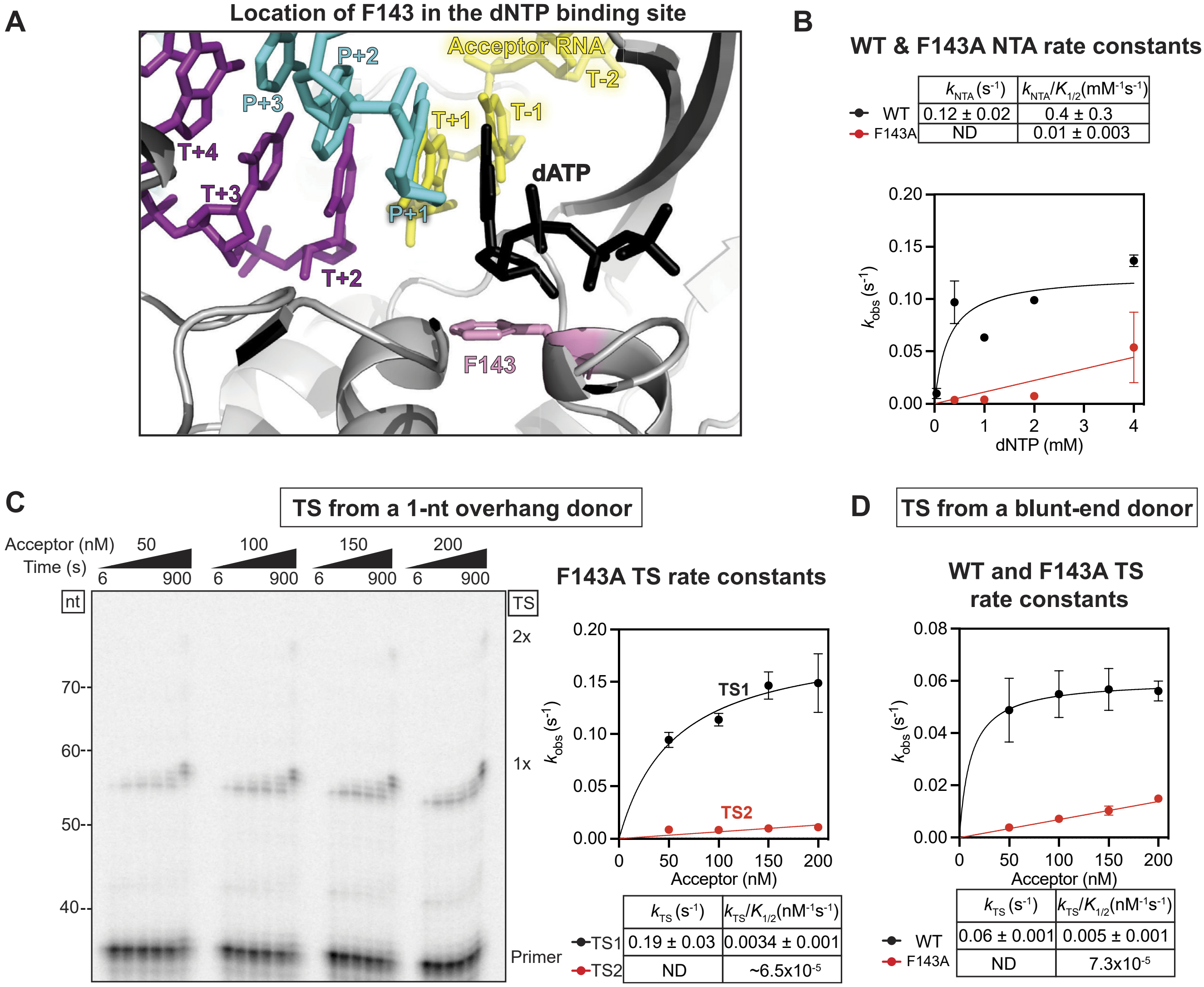

	k_{NTA} (s^{-1})	$k_{NTA}/K_{1/2}$(mM^{-1}s^{-1})
WT	0.12 ± 0.02	0.4 ± 0.3
F143A	ND	0.01 ± 0.003

	k_{TS} (s^{-1})	$k_{TS}/K_{1/2}$(nM^{-1}s^{-1})
TS1	0.19 ± 0.03	0.0034 ± 0.001
TS2	ND	~6.5x10^{-5}

	k_{TS} (s^{-1})	$k_{TS}/K_{1/2}$(nM^{-1}s^{-1})
WT	0.06 ± 0.001	0.005 ± 0.001
F143A	ND	7.3x10^{-5}

Figure 6. The effect of the F143A mutation on nontemplated nucleotide addition and template switching (TS) by GsI-IIC RT. *A*, close-up view of the dNTP-binding site showing F143 (*pink stick*) pi stacking with the ribose of the incoming dATP (*black stick*). Nucleic acids are colored as in Figure 1, *A* and *B*. *B*, NTA reactions for WT and F143A mutant GsI-IIC RT as a function of dNTP concentrations. The reactions were performed with blunt-end RNA template–DNA primer duplex of the same sequence as that used for TS but lacking the 1-nt 3′-DNA overhang and under the same reaction conditions as those used for TS in Figure 3. The plot shows k_{obs} as a function of dNTP concentration fit by a hyperbolic equation to obtain the maximal rate constant k_{NTA} and the second-order rate constant $k_{NTA}/K_{1/2}$ values. Each rate constant determination was performed at least twice, and a representative gel is shown in Figure S6*A*. The *error bars* in the plot show the standard error of the mean, and the uncertainties in the k_{NTA} and $k_{NTA}/K_{1/2}$ values in the table above indicate the standard error of the fit. The 0.04 mM concentration for F143A was omitted because of poor fitting due to low amounts of product formation. *C*, TS reactions of the F143A mutant from a 1-nt 3′-DNA overhang RNA template–DNA primer duplex. Reactions were performed as described in Figure 3. The numbers to the left of the gel indicate the length and position of size markers (5′-^{32}P-labeled single-stranded DNA ladder; ss20 DNA Ladder; Simplex Sciences) run in a parallel lane of the same gel. Each rate constant determination was performed at least twice. The plot to the right shows the observed rate constant k_{obs} as a function of acceptor RNA concentration for the initial template switch from the donor duplex (TS1) and the second template switch from the 5′ end of first RNA template to the 3′ end of a second RNA template (TS2). The data points were fit by a hyperbolic function. *D*, TS of WT and F143A mutant GsI-IIC RT from a blunt-end duplex. TS reactions were done as described in Figure 3. Each rate constant determination was performed three times, and a representative gel is shown in Figure 5*B*. The plot shows k_{obs} as a function of acceptor concentration fit by a hyperbolic equation to obtain the maximal rate constant k_{TS} and the second-order rate constant $k_{TS}/K_{1/2}$, as indicated in the inset table. In panels *C* and *D*, the error bars in the plots show the standard error of the mean, and the uncertainties in the tables below each plot indicate the standard error of the fit. RT, reverse transcriptase.

of premature stops and a relatively small decrease in rate (10 nt/s compared with 20 nt/s for WT at 4 mM dNTPs; Fig. S2 and Table 2).

Next, we measured the TS activity of F143A with a donor RNA template–DNA primer heteroduplex with a preformed 1-nt 3′-DNA overhang and increasing concentrations of acceptor RNA under our standard reaction conditions with 4 mM dNTPs. We found that the F143A mutant produced cDNA products at a rapid rate (k_{TS} = 0.19 ± 0.03 s^{-1}), reflecting that the first template switch from the donor duplex (TS1) was relatively unaffected, but with greatly reduced efficiency for the second template switch (TS2; $k_{TS}/K_{1/2}$ = ~6.5 × 10^{-5}; compare second template switch by F143A in the gel of Fig. 6*C* to WT in Fig. 3*B* and see later).

Finally, we anticipated that TS from a blunt-end donor would be strongly decreased by the F143A mutation with kinetic parameters similar to that of its second template switch from a 1-nt overhang substrate. As seen in Figure 6*D*, this was indeed the case, with TS from a blunt-end duplex by F143A showing an ~70-fold decrease in $k_{TS}/K_{1/2}$ compared with WT ($k_{TS}/K_{1/2}$ of 0.005 ± 0.001 for WT and 7.3 × 10^{-5} nM^{-1} s^{-1} for F143A; Fig. S6*B* and Table 2). Collectively, our results show that the F143A mutation had at most a small effect on the first template switch from a donor RNA template–DNA primer heteroduplex with 4 mM dNTPs but strongly inhibited multiple end-to-end template switches, which depend upon NTA to produce a single-nucleotide overhang (27).

Together, our results indicate that the F143A mutation weakens binding of an unpaired dNTP at the RT active site, thereby decreasing NTA activity. Although the F143A mutation may also weaken dNTP binding during cDNA synthesis, there was no decrease in the amplitude and only a relatively small decrease (twofold) in the rate (nt/s) of PE at the standard concentration of 4 mM dNTPs (Fig. S2 and Table 2). These results likely reflect that when the incoming dNTP can base pair with a templating nucleotide, 4 mM dNTP is saturating for the WT enzyme and nearly saturating for the mutant. Thus, under these conditions, the F143A mutation selectively inhibits NTA activity.

The F143A mutation decreases secondary template switches in RNA-Seq

TS from an RNA template–DNA primer duplex similar to that in the previous experiments but with a 1-nt 3′-DNA overhang that is an equimolar mix of all four nucleotides (denoted N) is employed in a high-throughput RNA-Seq method called TGIRT-Seq to initiate reverse transcription at the 3′ end of target RNAs with concomitant attachment of an RNA-Seq adapter to the 5′ end of a cDNA (Fig. 7*A*; (34–36)). A second RNA-Seq adapter is then added to the 3′ end of the completed cDNA by a single-stranded DNA ligation followed by minimal PCR amplification to generate the final TGIRT-Seq library for sequencing (Fig. 7*A*). For this method, it is desirable to maximize the efficiency of the initial template switch from donor duplex with a preformed 1-nt 3′-DNA overhang used for RNA-Seq adapter addition, whereas decreasing secondary template switches from the 3′ end of the completed cDNA, which result in chimeric reads that are typically discarded. The problem of multiple sequential template switches is most pronounced for TGIRT-Seq of size-selected short RNAs, such as miRNAs (23, 36). Although secondary template switches in TGIRT-Seq can be suppressed by a high salt concentration (450 mM NaCl), high salt also decreases the efficiency of TS from the initial starter duplex (35), resulting in a lower yield of library product. A recently introduced modification of the TGIRT-Seq method using a lower salt concentration (200 mM NaCl) for sequencing of human plasma RNAs resulted in <5% soft clipped or discordant read pairs that could include secondary TS (37), a manageable number but one that it would still be desirable to decrease further, as well as enable use of even lower salt concentrations to further increase the efficiency of the initial TS step.

To test the feasibility of using the F143A mutation to decrease the frequency of secondary template switches in TGIRT-Seq, we constructed TGIRT-Seq libraries with WT and F143A GsI-IIC RTs using the protocol outlined in Figure 7*A* in reaction medium containing 200 mM NaCl under conditions designed to exacerbate the number of secondary template switches, including the use of a very short 24-nt acceptor RNA with three randomized 3′ nucleotides (denoted NNN) to enable base pairing of different nucleotides added by NTA to the 3′ end of completed cDNAs (Fig. 7*A*). Bioanalyzer traces of the final TGIRT-Seq libraries after PCR amplification showed that F143A mutation substantially decreased the proportion of secondary template switches compared with the WT enzyme and that this decrease was more pronounced at 0.4 mM than at 4 mM dNTP (Fig. 7*B*), as expected from the aforementioned experiments comparing the efficiency of the reaction at subsaturating and near saturating dNTP concentrations for the mutant (Fig. 6).

Sequencing of the TGIRT-Seq library on an Illumina MiSeq instrument showed that 68.5% of the reads obtained with the F143A mutant at the lower dNTP concentration were free of multiple template switches compared with only 13% for the WT enzyme at either dNTP concentration and 25% for the F143A mutant at the higher dNTP concentration (Fig. 7*C*). The F143A mutation did not increase the frequency of base substitutions or indels above the composite error rate for TGIRT-Seq library preparation, oligonucleotide synthesis, PCR, and sequencing (Table S2). Because we used an acceptor RNA with randomized 3′ ends and because NTA still occurs to the 3′ end of the final cDNA synthesized after multiple template switches, the TGIRT-Seq datasets could also be used to assess the effect of the F143A mutation on nucleotide preferences for both NTA and acceptor to acceptor (A–A) TS. Notably, the F143A mutation led to a marked decrease in the proportion of G residues for the first NTA at both dNTP concentrations (Fig. 7*D*) and a concomitant decrease in secondary TS to acceptors with a complementary 3′ C residue (Fig. 7*E*). Collectively, these findings indicate that the F143A mutation in combination with lower dNTP concentrations may be useful for decreasing multiple template switches in TGIRT-Seq. In addition, because F143 corresponds to a conserved aromatic residue in the dNTP-binding site of all RTs, our findings suggest that mutations at this position may be generally useful for optimizing the number and composition of NTAs by retroviral and other RTs for SMART-Seq and other RNA-Seq applications.

Reversible binding of acceptor RNAs within the TS pocket and effect of RNA length

We hypothesized that the binding of the acceptor RNA within the TS pocket of GsI-IIC RT might be highly reversible, so that a mismatched acceptor whose 3′ end is not complementary to the 1-nt DNA overhang could dissociate rapidly, whereas a matched acceptor with a complementary 3′ end might dissociate more slowly, enabling it to be used preferentially upon addition of dNTPs. To test this hypothesis, we probed whether the complex formed after binding an acceptor with a 3′ nucleotide complementary to the 1-nt DNA overhang is committed to extension or could exchange rapidly with an acceptor RNA from solution. In these experiments, we preincubated GsI-IIC RT with a saturating concentration of a 21-

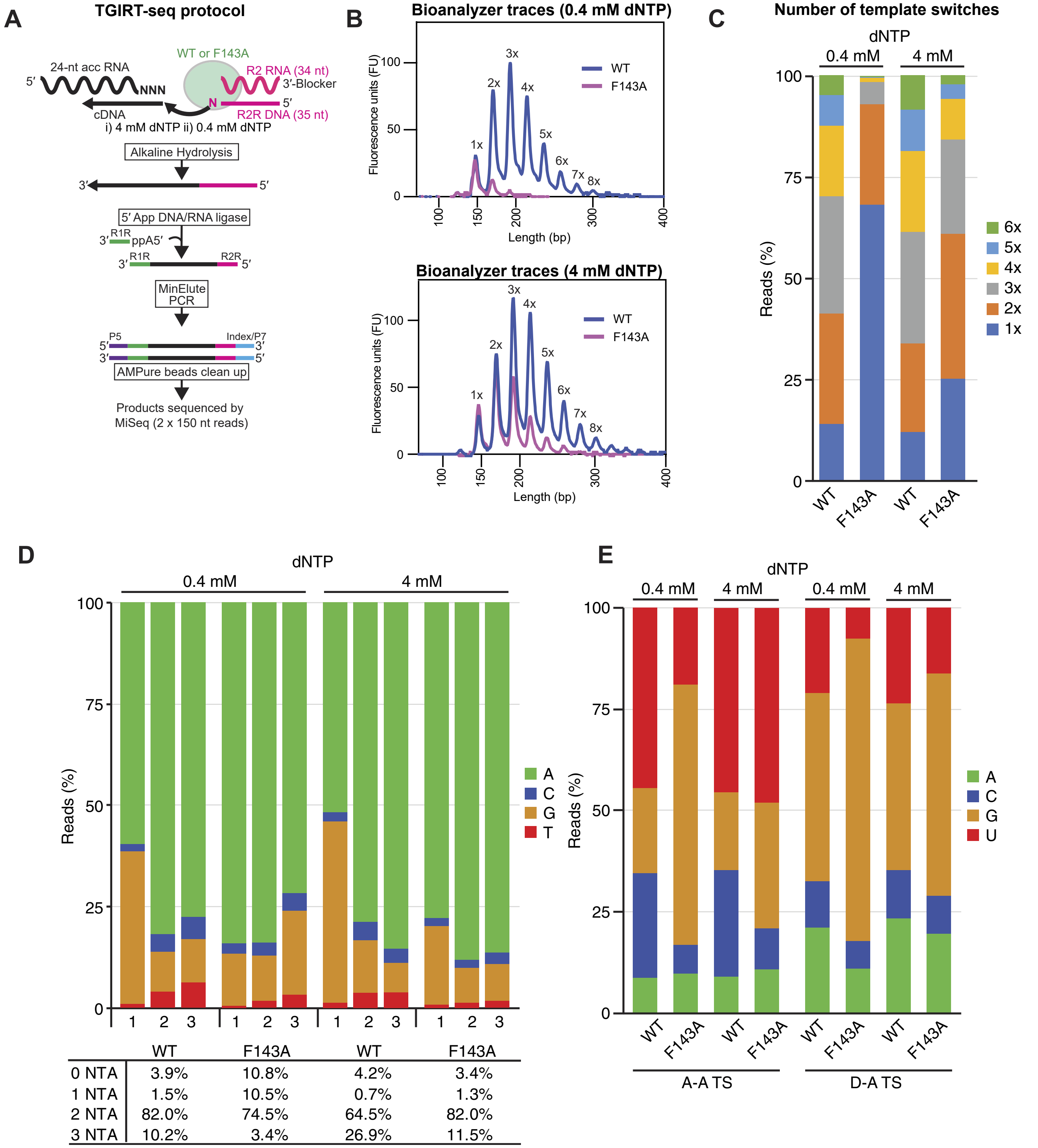

	WT	F143A	WT	F143A
0 NTA	3.9%	10.8%	4.2%	3.4%
1 NTA	1.5%	10.5%	0.7%	1.3%
2 NTA	82.0%	74.5%	64.5%	82.0%
3 NTA	10.2%	3.4%	26.9%	11.5%

Figure 7. The F134A mutation decreases secondary template switches in TGIRT-Seq. *A*, outline of the RNA-Seq workflow. Template-switching reactions using WT or F143A GsI-IIC RTs were performed with an unlabeled starter duplex with a 1-nt 3′-DNA primer overhang that was an equimolar mixture of A, C, G, and T residues (denoted N) and a 24-nt acceptor RNA of which each of the last three nucleotides was an equimolar mixture of A, C, G, and U residues (denoted N). After a 30-min preincubation, reactions were initiated by adding dNTPs, incubated at 60 °C for 15 min, and terminated by adding NaOH and heating to 95 °C for 3 min. Complementary DNA products were cleaned up by using a MinElute column (Qiagen) and then ligated to a 5′-adenylated R1R adapter using Thermostable 5′ App DNA/RNA Ligase (New England Biolabs). After another MinElute clean up, Illumina RNA-Seq capture sites (P5 and P7) and indices were added by PCR, and the resulting libraries were cleaned up by using AMPure XP beads (Beckman Coulter) prior to sequencing on an Illumina MiSeq version 2 to obtain 150-nt paired-end reads. *B*, bioanalyzer (Agilent; High Sensitivity DNA chip) traces of TGIRT-Seq libraries prepared *via* template switching at 0.4 and 4 mM dNTPs to the 24-nt acceptor RNA. The lengths indicated on the *x*-axis are those of internal DNA size markers, which were omitted from the trace for clarity. *C*, *stacked bar graphs* show the percentages of reads containing a single template switch from the starter duplex (1×) or multiple template switches from the 5′ end of one RNA template to the 3′ end of another (2× to 6×) in TGIRT-Seq datasets obtained with WT GsI-IIC RT and the F143A mutant at 0.4 or 4 mM dNTPs. *D*, *stacked bar graphs* showing the proportions of different nucleotides for the first, second, and third nontemplated-nucleotide additions at the 3′ end of the final complementary DNA synthesized after the last template switch in TGIRT-Seq datasets obtained

nt acceptor RNA and a donor template–primer duplex with a complementary 1-nt 3′-DNA overhang for 30 min to allow binding of the acceptor. We then initiated reverse transcription by adding dNTPs, with or without a 20-fold excess of a competitor 34-nt acceptor (Fig. 8*A*, *top*). To preclude sequence biases for binding within the TS pocket from influencing the experiment, the longer acceptor had the same 21-nt 3′ sequence as the shorter acceptor and differed only by the extra nucleotides at its 5′ end. Indeed, we found that TS occurred predominantly to the competitor 34-nt acceptor (Fig. 8*A*, *left lanes*), indicating that despite the potential for base pairing with the 1-nt DNA overhang, the 21-nt acceptor binds reversibly, dissociating faster than dNTP binding and extension.

Surprisingly, in a reciprocal experiment, in which GsI-IIC RT was preincubated with the 34-nt acceptor RNA and the donor duplex for 30 min before adding dNTPs with a 20-fold molar excess of 21-nt acceptor, only ~50% of the TS product switched to the shorter 21-nt acceptor (Fig. 8*A*, *right lanes*). Although this result could have indicated that the complex formed with the 34-nt acceptor is equally likely to dissociate or go on to chain extension, it was also possible that the 34-nt acceptor RNA binds preferentially from solution, even though both acceptors have identical 3′-end sequences.

To distinguish these possibilities, we performed an additional experiment in which both the longer and shorter acceptors were added together in different ratios along with dNTPs to initiate reverse transcription (Fig. 8*B*). This experiment showed that when the 34-nt acceptor was present in excess from the beginning, it was used exclusively for TS, whereas when the 21-nt acceptor was present in excess from the beginning, the 34-nt was still present in >50% of the TS products. This preferential binding of the longer acceptor RNA indicates that its 5′ end can interact with additional sites on the RT outside the TS pocket, likely patches of basic residues on the outer surface of the protein that are used for binding group II intron RNAs for RNA splicing and retrohoming (24) (Fig. 8*C*). These findings account for a previously observed size bias against RNAs <60 nt in heterogeneously sized RNA preparations in TGIRT-Seq using GsI-IIC RT (37, 38) and suggest approaches for mitigating this bias by mutating basic surface residues that are not required for reverse transcription.

Discussion

Here, we determined a crystal structure of a group II intron RT TS complex with synthetic oligonucleotides representing an acceptor RNA and a donor RNA template–cDNA duplex after NTA to form a complementary 1-nt 3′-DNA overhang. The structure showed that the 3′ end of the acceptor RNA binds in a pocket formed by the NTE and fingertips loop with its 3′ nucleotide base paired to the 1-nt DNA overhang and its penultimate nucleotide base paired to an incoming dNTP at the RT active site. This TS pocket is ordinarily occupied by upstream regions of a continuous RNA template but would become vacant when the RT reaches the 5′ end of an RNA template or dissociates from a broken or damaged template, enabling TS to the 3′ end of a new acceptor RNA template for the continuation of cDNA synthesis.

Globally, the structure of the GsI-IIC RT TS complex is similar to that of GsI-IIC RT bound to a continuous RNA template–DNA primer duplex, the major differences detectable at this resolution being the lack of a phosphate in the gap between the 3′ end of the acceptor and 5′ end of the donor templates and a small shift in the position of N23, possibly reflecting the lack of that phosphate. The NTE, which forms part of the TS pocket, is a common feature of non-LTR-retroelement RTs and viral RdRPs but is lacking and presumed to have been lost from retroviral RTs. A critical part of the NTE for TS is the RT0 loop, a structured polypeptide linker that in GsI-IIC RT connects the two bent α-helices of the NTE and forms a lid over the RNA template backbone (Figs. 2 and 4). The RT0 loop sequence is conserved in group II intron RTs and partially conserved in non-LTR-retroelement RTs (Fig. 1*C*). In GsI-IIC RT, conserved small amino acids at the N terminus of the RT0 loop (G25 and A26) allow close approach and interaction of this portion of the lid with the RNA acceptor phosphate backbone. Most of the remaining conserved amino acids in the loop are hydrophobic residues involved in packing interactions with the fingers that anchor the middle and C-terminal end of the structured loop. In high-resolution crystal structures of two closely related apo-group II intron RTs (29), the RT0 loop adopted the same conformation utilizing the same conserved interactions. Furthermore, cryo-EM structures of the more distantly related Ll.LtrB and TeI4h group II intron RTs in complexes with group II intron RNA support a similar location for the lid and a packed RT0 loop in the absence of reverse transcription substrates (28, 30). Collectively, these findings indicate that the structured RT0 loop conformation as seen in GsI-IIC RT is not dependent upon the presence of a nucleic acid substrate in the TS pocket. In addition, the RT0 loop has the same configuration in the TS structure and the continuous structure, suggesting that it may not undergo large conformational changes during TS.

Because the 3′ end of the RNA acceptor is bound and held in place primarily by polypeptide backbone interactions with the RT0 loop lid, we sought to disrupt the structure of the lid to test whether acceptor binding would be affected. We found that the mutation 23-31/4G, in which residues 23 to 31 were replaced by four glycines, resulting in a shorter loop and ablating a critical anchoring interaction of the loop with the fingers, strongly inhibited TS activity but had no detectable effect on PE activity, indicating that maintaining the proper conformation of the lid is critical for acceptor RNA binding. The binding of the lid to the RNA acceptor may constrain

with WT GsI-IIC RT and the F143A mutant at 0.4 and 4 mM dNTPs. The table below shows the percentages of 0, 1, 2, or 3 nt NTAs for each condition. *E, stacked bar graphs* showing nucleotide frequencies of the 3′-terminal nucleotide of the acceptor RNA in TGIRT-Seq datasets obtained with WT GsI-IIC RT and the F143A mutant at 0.4 and 4 mM dNTPs for acceptor to acceptor (A–A) and starter duplex to acceptor (D–A) template switches. RT, reverse transcriptase; TGIRT, thermostable group II intron reverse transcriptase.

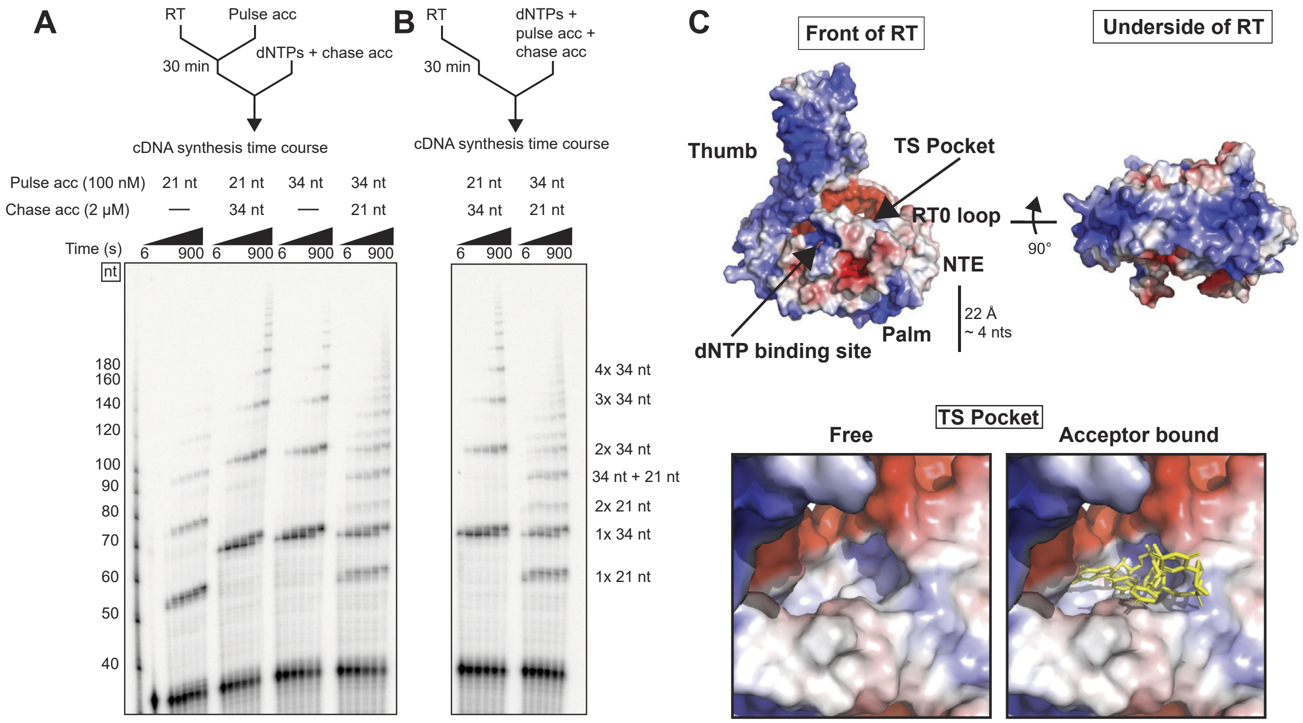

Figure 8. Template switching (TS) by GsI-IIC RT favors a longer acceptor RNA. *A*, schematic of the experiment. WT GsI-IIC RT (200 nM) in complex with a labeled 20 nM 1-nt 3′-DNA overhang starter duplex was incubated with 100 nM of a 21- or 34-nt acceptor RNA for 30 min, after which the reaction was started by adding 4 mM dNTPs and an excess (2 μM) of a reciprocal 34- or 21-nt acceptor RNA. *B*, WT GsI-IIC RT (200 nM) in complex with a labeled 20 nM 1-nt 3′-DNA overhang starter duplex was incubated for 30 min, after which the reaction was started by adding 4 mM total dNTPs, 100 nM of a 21- or 34-nt acceptor RNA, and 2 μM of a 34-nt or 21-nt acceptor RNA. Reaction time courses were analyzed by electrophoresis in a denaturing 6% polyacrylamide gel. The numbers to the left of the gel indicate the lengths of size markers (5′-^{32}P-labeled single-stranded DNA ladder; ss20 DNA Ladder; Simplex Sciences) run in a parallel lane of the same gel. *C*, electrostatic potential surface representation of GsI-IIC RT created using the APBS Electrostatics plugin for Pymol. Electropositive regions are *blue*, and electronegative regions are *red*. In the front view (*top left*), the entrance of the TS pocket is indicated by an *arrow*, and a scale bar is included to give a sense of the distance that could be reached from the 5′ end of an acceptor RNA extending outside the TS pocket. Close-up views of the TS pocket without and with the bound 5-nt acceptor RNA in the crystal structure (*yellow stick*) are shown at the bottom. RT, reverse transcriptase.

mobility at its 3′ end and facilitate its alignment for TS. After acceptor RNA binding, the shortened glycine-rich lid in the 23-31/4G mutant adopts a conformation that does not impede reverse transcription.

Most of the remainder of the binding surface for the acceptor RNA in the TS pocket is formed by the fingertips loop, which is a conserved β-hairpin that is present in all RTs and harbors the two essential basic catalytic residues (K69 and R75 in GsI-IIC RT) on the surface that faces the polymerase active site (31). In known structures of RTs that contain a 5′-RNA overhang, the opposite face of the fingertips loop binds to the single-stranded RNA template region that awaits copying by using a group of hydrophobic residues projecting outward from the β-hairpin (39, 40). In the TS structure, the acceptor RNA binds to this same surface of the fingertips loop *via* a series of aliphatic residues that are conserved in other group II intron and non-LTR-retroelement RTs (Fig. 1*C*). We found that mutations in L77 and I79 strongly inhibited TS activity, while only slightly slowing PE. These residues comprise the primary binding surface for the T-1 and T-2 nucleotides of the acceptor RNA and collectively contact most of the fingertips loop-facing surface of the ribose rings and bases of these nucleotides. The finding that mutations in these residues strongly inhibited TS but not PE indicates that they make a proportionally greater contribution to binding an acceptor RNA for TS than for binding the upstream region of a continuous RNA template, which is covalently attached to the polymerized duplex.

In the TS structure, the RNA acceptor binds to a conformation of the fingertips loop that is engaged with the dNTP *via* the catalytic basic residues and poised for reverse transcription. In group II intron RT structures that do not contain substrate, the fingertips loop is observed in a more open conformation, although these structures are also influenced by the presence of the intron RNA (28, 30) or crystal packing interactions (29). Presumably, though, the fingertips loop must be somewhat dynamic to allow binding of a new dNTP after each polymerization cycle. In the open conformation, the catalytic basic residues are out of reach of the dNTP, and a portion of the RNA acceptor binding site would be disrupted. Our structure suggests that binding of dNTP and RNA acceptor could work in concert to promote reverse transcription during a template switch by stabilizing the closed conformation of the fingertips loop.

We found previously that efficient TS is dependent upon base pairing of the 3′ nucleotide of the acceptor with a 1-nt 3′-DNA overhang representing NTA of a single nucleotide to the 3′ end of the cDNA and that longer overhangs resulting from multiple NTAs were progressively less efficient, possibly reflecting the difficulty of matching two base pairs within the narrow confines of the donor duplex binding cleft prior to initiating cDNA synthesis (27). Here, we identified a mutation in a phenylalanine residue (F143A), which strongly inhibited NTA, while retaining relatively high PE activity (Figs. 6 and S2). F143 corresponds to a conserved aromatic residue (F or Y) that is present in all RTs and forms a pi-stacking interaction with the deoxyribose of the incoming dNTP, while also serving to exclude rNTPs from the active site *via* a steric clash with the 2′ OH of the rNTP ribose (24, 33, 39). During NTA, when the incoming dNTP is not held in place by base pairing with a templating RNA nucleotide, the F143A mutant displays substantially decreased activity even at high dNTP concentrations, when compared with PE for which dNTP concentrations remain close to saturating (compare Fig. S2 with Figs. 6*B* and S6*A*). Our finding that this mutation inhibited TS from the 5′ end of a reverse transcribed template or a blunt-end donor RNA–DNA duplex (Fig. 6, *C* and *D*), but not from a donor RNA–DNA duplex with a preformed 1-nt DNA overhang, confirms the necessity of NTA after the completion of cDNA synthesis for TS to a new acceptor.

Previous studies showed that the specificity of TS by GsI-IIC RT is dictated largely by base pairing of the 3′ end of the acceptor to the 1-nt 3′-DNA overhang of the donor, with no sequence biases for other positions at the 3′ end of the acceptor RNA (23, 34, 36). The TS structure indicates that this lack of sequence bias reflects that binding of the acceptor within the TS pocket is dependent largely upon either hydrophobic interactions or interactions of the protein with the phosphate backbone or ribose 2′ OH, with no H-bond interactions to specific bases. This weak binding of the acceptor enables its rapid dissociation in the absence of a base pair with a complementary 1-nt 3′-DNA primer overhang added by NTA or provided by a starter duplex for RNA-Seq.

Remarkably, despite being dictated by only a single base pair, the TS reaction of GsI-IIC RT has high specificity, with RNA-Seq showing 97.5 to 99.7% precise junctions depending upon the base pair (27). Our structure and kinetic analysis suggest that this high specificity reflects that after base pairing of the 3′ nucleotide of the acceptor to the 1-nt DNA overhang, a second base-pairing interaction between the templating RNA base and the incoming dNTP accompanied by a conformational change involving the fingertips loop results in initiation of reverse transcription, making the reaction with the matched acceptor irreversible.

Several of our findings are relevant to the use of group II intron RTs for RNA-Seq. First, the F143A mutation, which inhibits NTA and secondary template switches (Figs. 6 and 7), provides a new tool for decreasing artifactual fusion reads, making it easier to identify *bona fide* hybrid transcripts, such as those resulting from chromosome rearrangements in cancer and other diseases. The use of this mutation would not only decrease reliance on high salt concentrations, which have been used previously to decrease secondary template switches, but also decrease the efficiency of the initial template switch used for RNA-Seq adapter addition from a 1-nt 3′ overhang duplex (35). We also found that the F143A mutation changes nucleotide preferences for NTA and concomitantly changes nucleotide preferences for TS from the 5′ end of one template to the 3′ end of another, which are dependent upon base pairing of the nucleotides added by NTA to the 3′ end of the new acceptor (Fig. 7, *D* and *E*). As F143 corresponds to a conserved aromatic found in all RTs (33), engineering of this residue to ablate, change, or optimize the pi-stacking interaction to modulate NTA might also be possible for retroviral and other RTs employed in RNA-Seq methods such as SMART-Seq. Finally, our finding that longer RNAs outcompete shorter RNAs with identical 3′ ends indicates that the efficiency of TS can be influenced by the binding of upstream regions of longer acceptor RNAs to secondary sites outside the TS pocket and accounts for the previously observed TGIRT-III bias against miRNA-sized RNAs in heterogeneously sized RNA preparations (36, 38). These secondary binding sites likely include patches of basic residues on the surface of group II intron RTs that are used for binding group II intron RNAs for RNA splicing and reverse splicing in retrohoming. These basic patches are not required for reverse transcription and thus should be dispensable and relatively easy to remove for RNA-Seq applications (41, 42).

Although all non-LTR-retroelement RTs have an NTE, both its structure and the degree of conservation of the RT0 loop vary in different enzymes. In group II intron RTs, the NTE appears to be predominantly α-helical, but the arrangement of the helices varies in known structures of group II intron RTs (28, 30). The predicted RT0 loops of the three non-LTR-retroelement RTs in Figure 1*C* share only a glycine residue and an aspartate residue (homologous to D30 in GsI-IIC RT), which appeared largely dispensable for TS (Fig. 1*C*) (24). Despite this lack of sequence conservation, mutating the RT0 loop in the *Bombyx mori* R2 element RT abrogated TS activity (43), similar to our findings for GsI-IIC RT. In contrast to the RT0 loop sequence, the hydrophobic and aliphatic residues that contribute to acceptor RNA binding in the fingertips region of the TS pocket of GsI-IIC RT are well conserved in non-LTR-retroelement RTs (Fig. 1*C*). Collectively, these findings together with other previous biochemical analyses of TS by the R2 element RT (44, 45) suggest that group II intron and non-LTR-retroelement RTs use fundamentally similar TS mechanisms but that the structure of the NTE and TS pocket can diverge, possibly to accommodate the life cycle of different retroelements.

An example of such accommodation is provided by *Neurospora* spp. mitochondrial retroplasmids, which encode RTs that have a predominantly helical NTE domain and an RT0 loop region with no recognizable sequence similarity to that of group II intron RTs (46). These retroplasmid RTs use TS to a 3′ CCA sequence to generate concatemeric DNAs that are resolved by intramolecular DNA recombination to generate circular plasmid DNAs (47, 48). They also template switch to the 3′ end of tRNAs to generate chimeric plasmids for which the integrated tRNA sequence confers a replicative advantage when integrated into plasmid DNA (49). RT recognition of the 3′ CCA could occur within the TS pocket, possibly involving the RT0 loop, which contains multiple aromatic Phe, Tyr, and Trp residues that could mediate recognition of specific nucleotides (46). In addition to the 3′ CCA, the retroplasmid RT also binds the acceptor stem cognate of a 3′ tRNA-like secondary structure of the plasmid transcript (47), possibly using surface residues outside the TS pocket, as suggested for the binding of oligonucleotides with longer 5′ ends by GsI-IIC RT (Fig. 8*B*).

We found that group II intron RTs utilize the same binding surface for both upstream region of continuous RNA templates during PE and acceptor binding during TS, with the acceptor sandwiched between the NTE–RT0 loop on one side and the fingertips loop on the other side (Fig. 9*A*). Retroviral and LTR-retrotransposon RTs, which lack an NTE with an RT0 loop, perform analogous TS termed clamping, yet typically require at least two base pairs of primer–acceptor overlap for efficiency instead of a single base pair as for group II intron RTs (19, 20). Based on our findings for GsI-IIC RT, modeling

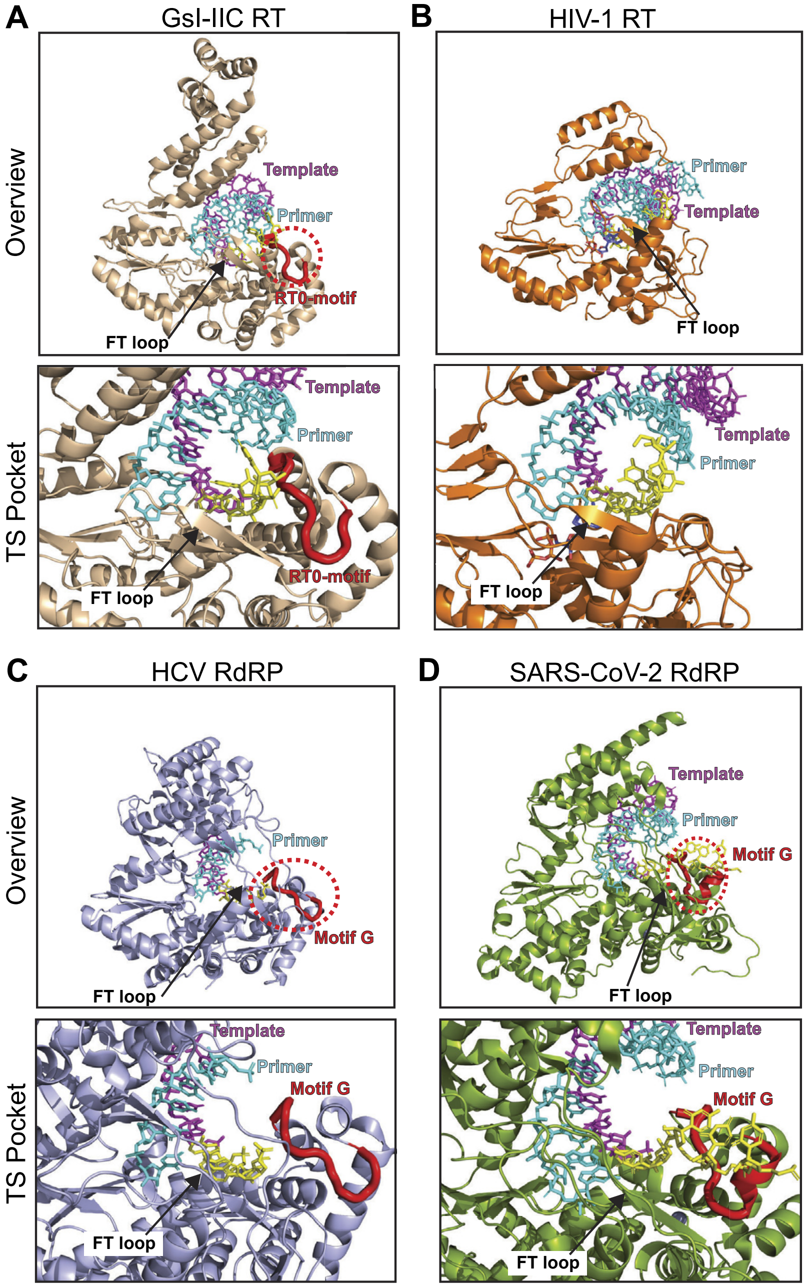

Figure 9. Comparison of upstream template RNA-binding regions that comprise the template-switching pocket of GsI-IIC RT compared with the same regions of HIV-1 RT and viral RdRPs. *A*, GsI-IIC RT (PDB ID: 6AR1 (24), *tan*); *B*, HIV-1 RT (PDB ID: 4PQU (39), amino acids 1–312 showing the RT and thumb domains, *orange*); *C*, HCV RdRP (PDB ID: 4WTA (56), *light blue*); *D*, SARS-CoV-2 RdRP (PDB ID: 72CK (57) with the nonhomologous N-terminal amino acids 1–356 removed, *light green*). For each enzyme, *cartoon representations* are shown as overviews (*top*) or zoomed in on the putative template-switching pocket region (*bottom*). Primer strands are cyan (*stick representation*), and RNA strands are purple (*stick representation*) in all three proteins. The RT0 loop and the RT0 loop cognate "motif G" in RdRPs are highlighted and shown in *red carton* within a *dotted red circle*. The fingertips (FT) loop is indicated by an *arrow*. Structural alignments were done using Coot (67). HCV, hepatitis C virus; PDB, Protein Data Bank; RdRP, RNA-dependent RNA polymerase; RT, reverse transcriptase; SARS-CoV-2, severe acute respiratory syndrome coronavirus 2.

suggests that the acceptor-binding surface for retroviral RTs consists of residues in the palm near the primer–acceptor overlap and hydrophobic residues in the fingertips loop in homologous positions to those found in GsI-IIC RT (Fig. 9*B*) (19, 20). The lack of any protein structure corresponding to the NTE–RT0 loop to sandwich the RNA acceptor may explain the necessity of at least one additional base pair and a larger binding surface on the palm for efficient clamping by retroviral RTs compared with group II intron RTs. Retroviral RTs can also template switch *via* strand transfer, but this process is more akin to PE, as the donor template is degraded by RNase H, and the remaining cDNA base pairs to a complementary template (18).

Finally, viral RdRPs, which are thought to be evolutionary ancestors of RTs, can template switch by an end-to-end mechanism analogous to clamping as well as by strand transfers that produce physiologically relevant subgenomic RNAs and enable recombination between viral RNA templates (50–55). Structures of well-studied RdRPs, including hepatitis C virus RdRP (PDB ID: 4WTA (56)) and severe acute respiratory syndrome coronavirus 2 RdRP (PDB ID: 72CK (57)) (Fig. 9, *C* and *D*; see also PDB ID: 2E9T (58), PDB ID: 5TSN (59), and PDB ID: 1S48 (60)), show a putative TS pocket composed of an RT0 loop cognate (termed motif G in RdRPs) and the fingertips loop on either side (61). The TS pocket homology between RdRPs and group II intron RTs suggests a common mechanism for binding the acceptor RNA template. Furthermore, small numbers of extra nucleotides at TS junctions for some viruses suggest a role for NTA similar to the mechanisms of retroviral and group II intron RT clamping (27, 52). However, RdRPs lack an aromatic residue corresponding to the NTA-facilitating F143 in GsI-IIC RT, which would sterically clash with the 2′ OH on the ribose ring of rNTPs, and instead use hydrogen bonds to the 2′ OH to impart selectivity for rNTPs (33, 62). In addition, in hepatitis C virus RdRP, the mutation D225A in a residue that is part of a conserved hydrogen-bonding network that stabilizes the ASG loop, inhibits TS but not PE or NTA, possibly by affecting interaction of the ASG loop with the acceptor RNA (54). As with viral RdRPs, group II intron RTs typically possess homologs of both D225 (D144 in GsI-IIC RT) and the ASG loop (PQG loop in GsI-IIC RT with G192 of the PQG loop contacting T-1 of the acceptor; Fig. 1*B*), suggesting future avenues for investigating the effect of mutations in these residues on TS activity in these polymerase families.

Experimental procedures

DNA and RNA oligonucleotides

The DNA and RNA oligonucleotides used in this work are listed in Table S1. Most were purchased in RNase-free and HPLC-purified form from Integrated DNA Technologies. For biochemical assays, the R2R and PE DNA primers (100 pmol) were labeled with [γ-^{32}P]ATP (125 pmol; 6000 Ci/mmol; 150 μCi/μl; PerkinElmer Life Sciences) by incubating the DNA with T4 polynucleotide kinase (10 units; New England Biolabs) in the reaction medium provided by the supplier for 30 min at 37 °C. A typical 10-μl reaction was then diluted to 40 μl with double-distilled water and extracted with an equal volume of phenol/chloroform/isoamyl alcohol (25:24:1). Unincorporated nucleotides were removed from the aqueous phase by using a P-30 Microspin column (RNase Free; Bio-Rad), and the oligonucleotide concentration was measured by using a Qubit ssDNA assay kit (Thermo Fisher Scientific). The concentration of unlabeled oligonucleotides was determined by spectrophotometry using a NanoDrop 1000 (Thermo Fisher Scientific).

Expression and purification of GsI-IIC RT protein used in crystallography

GsI-IIC RT with a C-terminal 8× His tag was expressed from plasmid pET-14b GsI-IIC RT C-term 8xHis and purified by essentially the same methods described previously (24). A freshly transformed colony of *E. coli* BL21-CodonPLus (DE3)-RIPL cells (Agilent) was inoculated into 100 ml of LB medium containing ampicillin (50 μg/ml) and chloramphenicol (25 μg/ml) in a 250-ml Erlenmeyer flask and grown overnight with shaking at 37 °C. About 50 ml of this starter culture was then added to 1 l of LB medium containing ampicillin (50 μg/ml) in 4-l Erlenmeyer flasks and grown at 37 °C to an absorbance at 600 nm of 0.7 to 0.8, at which time protein expression was induced by adding 1 mM IPTG and incubating at 37 °C for 2 h. The cells were pelleted by centrifugation and stored at −80 °C overnight. After thawing on ice, the cells were lysed by sonication in 40 ml of buffer containing 100 mM NaCl, 20 mM Tris–HCl at pH 8.5, 10% glycerol, 5 mM imidazole, 0.1% β-mercaptoethanol, 0.2 mM PMSF, and one cOmplete EDTA-free protease inhibitor cocktail tablet (Roche), and the lysate was clarified by centrifugation at 30,000*g* for 60 min at 4 °C in a JA25.50 rotor in an Avanti J-E centrifuge (Beckman). The clarified lysate was then added to 10 ml of nickel–nitrilotriacetic acid agarose beads (Invitrogen) and incubated with rotation at 4 °C for 2 h. The beads were washed under gravity flow first with 250-ml wash buffer A (20 mM Tris–HCl at pH 8.5, 100 mM NaCl, 10% glycerol, 5 mM imidazole, and 0.1% β-mercaptoethanol) and then with 150-ml wash buffer B (20 ml Tris–HCl at pH 8.5, 100 mM NaCl, 10% glycerol, 50 mM imidazole, and 0.1% β-mercaptoethanol). The protein was then eluted by washing five times with 5 ml of elution buffer (20 mM Tris–HCl at pH 8.5, 100 mM NaCl, 10% glycerol, 250 mM imidazole, and 0.1% β-mercaptoethanol). Fractions were analyzed by SDS-PAGE, and those containing GsI-IIC RT were pooled and loaded onto a 5-ml heparin HP column (GE Healthcare) pre-equilibrated in heparin buffer A (20 mM Tris–HCl at pH 8.5, 100 mM NaCl, 10% glycerol, and 0.1% β-mercaptoethanol) at a flow rate of 1 ml/min. The column was washed with five column volumes (CVs) of heparin buffer A and eluted with a 10 CV linear gradient of heparin buffer A to 50% heparin buffer B (2 M NaCl, 20 mM Tris–HCl at pH 8.5, 10% glycerol, and 0.1% β-mercaptoethanol), after which a final 5 CV of 100% heparin buffer B was applied. Fractions containing GsI-IIC RT identified by SDS-PAGE were pooled and concentrated by incubating in 65% saturating ammonium sulfate and centrifuging the precipitated protein at 20,000*g* for 2 h at 4 °C. The resulting protein pellet was resuspended in crystallization buffer (500 mM NaCl, 20 mM Tris–HCl at pH 8.5, 10% glycerol, and 5 mM DTT) to a final concentration of ∼2 mg/ml.

Crystallization

For crystallization, an RNA–DNA starter duplex was formed by combining the single-stranded RNA template and DNA primer oligonucleotides, the latter ending with 3′ ddCTP, at a 1:1 molar ratio, heating to 82 °C for 2 min, and then slowly cooling to room temperature. The annealed starter duplex was then combined with GsI-IIC RT and a 5′-UUUUG acceptor RNA oligonucleotide at a molar ratio of 1:1.2:2 (protein:starter duplex:acceptor RNA). The crystallization buffer also contained 1 mM dATP and 10 mM $MgCl_2$. This mixture was incubated on ice for 30 min and centrifuged at 20,000*g* for 30 min at 4 °C. Crystals were grown by the hanging drop vapor diffusion method, with drops containing 0.5 μl of GsI-IIC RT/duplex/acceptor and 0.5 μl of well solution containing 0.1 M Hepes at pH 7.0 and 1.3 M sodium citrate tribasic dihydrate. Crystals grew as characteristic thin plates over the course of 1 to 2 weeks. Crystals were harvested with a cryoloop (Hampton Research) and immersed briefly in Al's oil (Hampton Research) before flash freezing in liquid nitrogen.

Data collection and processing

Diffraction data were collected at 100 K at the Advanced Light Source (ALS) on beamline 5.0.1. Images were integrated using the XDS package (63) and scaled with Aimless (64). Molecular replacement followed by rigid body refinement was carried out using a GsI-IIC RT model (PDB ID: 6AR3) with the dATP and the RNA acceptor removed. Refinement was carried out in Refmac5 with the twin law h+2*l, -k, -l, twin fraction = 0.5 applied (65). The R_{Free} set was chosen to match that of 6AR3. Data collection and refinement parameters are reported in Table 1. Composite omit maps were calculated using *comit* in the CCP4 suite with default parameters (66). The monomer composed of chains A (protein), B (DNA primer), C (RNA donor), and G (RNA acceptor) was used throughout this work for depictions and structural analysis because of better density than the other monomer.

Expression and purification of GsI-IIC RT proteins used in biochemical assays

GsI-IIC RT with an N-terminal maltose-binding protein tag to keep the protein soluble and stable in the absence of bound nucleic acids was expressed from plasmid pMRF–GsI-IIC RT (23). A freshly transformed colony of *E. coli* Rosetta 2 (DE3) cells (EMD Millipore) was inoculated into 1 l of LB medium containing ampicillin (50 μg/ml) and chloramphenicol (25 μg/ml) in a 4-l Erlenmeyer flask and grown overnight with shaking at 37 °C. About 50 ml of the starter culture was then added to 1 l of LB medium containing ampicillin (50 μg/ml) in one to six 4-l Erlenmeyer flasks and grown at 37 °C to an absorbance at 600 nm of 0.6 to 0.7, at which time protein expression was induced by adding 1 mM IPTG and incubating overnight with shaking at 19 °C. The cells were pelleted by centrifugation and stored at −80 °C overnight. After thawing on ice, the cells were lysed by sonication in 500 mM NaCl, 20 mM Tris–HCl at pH 7.5, 20% glycerol, 0.2 mM PMSF (Roche Applied Science), and one cOmplete EDTA-free protease inhibitor cocktail tablet (Roche), after which the lysate was clarified by centrifugation at 30,000*g* for 60 min at 4 °C in a JA 25.50 rotor in an Avanti J-E centrifuge (Beckman). Nucleic acids in the clarified lysate were precipitated by slowly adding polyethyleneimine with constant stirring in an ice bath to a final concentration of 0.4% and then centrifuging at 30,000*g* for 25 min at 4 °C in a JA 25.50 rotor (Beckman). GsI-IIC RT and other cellular proteins were then precipitated from the supernatant with 60% saturating ammonium sulfate, pelleted at 30,000*g* for 25 min at 4 °C in a JA 25.50 rotor (Beckman), and resuspended in 25 ml of A1 buffer (300 mM NaCl, 25 mM Tris–HCl at pH 7.5, and 10% glycerol). The protein mixture was then purified through two tandem 5-ml MBPTrap HP columns (GE Healthcare). After loading, the tandem column was washed with five CVs of A1 buffer, and the maltose-binding protein–tagged GsI-IIC RT was eluted with ten CVs of 500 mM NaCl, 25 mM Tris–HCl at pH 7.5, and 10% glycerol containing 10 mM maltose. The final fractions containing the RT were diluted to 200 mM NaCl, 20 mM Tris–HCl at pH 7.5, 10% glycerol, loaded onto a 5-ml HiTrap Heparin HP column (GE Healthcare), and eluted with a 12-CV gradient from buffer A1 to A2 (1.5 M NaCl, 25 mM Tris–HCl at pH 7.5, and 10% glycerol) taking 0.5-ml fractions. Fractions containing GsI-IIC RT were identified by SDS-PAGE, pooled, and concentrated using a 30 K centrifugation filter (Amicon). The concentrated protein was then dialyzed into 500 mM NaCl, 20 mM Tris–HCl at pH 7.5, 50% glycerol, and aliquots were flash frozen using liquid nitrogen and stored at −80 °C. Protein concentrations were determined by the Pierce BCA Protein Assay Kit (Thermo Fisher Scientific).

TS and nontemplated addition assays

TS reactions with GsI-IIC RT were carried out by using the previously described protocol with minor modifications (23). The RNA template–DNA primer starter duplex was based on that used for 3′-adapter addition in TGIRT-Seq (34) and consists of a 34-nt RNA oligonucleotide containing an Illumina R2 sequence (R2 RNA) with a 3′-blocking group (3SpC3; Integrated DNA Technologies; Table S1) annealed to a cDNA primer (R2R) that leaves either a blunt end or a single nucleotide 3′-DNA overhang end (Table S1). The oligonucleotides were mixed in 1× Tris–EDTA at a ratio of 1:1.2, annealed by heating to 82 °C for 2 min, and then slowly cooled to room temperature to yield a donor duplex concentration of 20 nM. Unless specified otherwise, reactions were done with 200 nM GsI-IIC RT, 20 nM R2 RNA–R2R DNA starter duplex, and various concentrations of acceptor oligonucleotide in 25 μl of reaction medium containing 200 mM NaCl, 5 mM $MgCl_2$, 20 mM Tris–HCl at pH 7.5, 5 mM fresh DTT, and an equimolar mix of 1 mM each of dATP, dCTP, dGTP, and dTTP (Promega) to give a total dNTP concentration of 4 mM. Reactions were set up with all components except dNTPs, preincubated for 30 min at room temperature, and initiated by adding 1 μl of 25 mM dNTPs (an equimolar mix of 25 mM dATP, dCTP, dGTP, and dTTP). Reactions were then incubated at 60 °C for times indicated in the legends to the figures and stopped by adding 2.5-μl portions to 7.5 μl of 0.25 M EDTA. The products were further processed by adding 0.5 μl of 5 N NaOH and heating to 95 °C for 3 min to degrade RNA and remove tightly bound GsI-IIC RT, followed by a cooling to room temperature and neutralization with 0.5 μl of 5 N HCl. After adding formamide loading dye (5 μl; 95% formamide, 0.025% xylene cyanol, 0.025% bromophenol blue, 10 mM Tris–HCl at pH 7.5, and 6.25 mM EDTA), the products were denatured by heating to 99 °C for 10 min and placed on ice prior to electrophoresis in a denaturing 6% polyacrylamide gel (7 M urea, 89 mM Tris borate, and 2 mM EDTA, and pH 8) at 65 W for 1.5 to 2 h. A 5′-labeled, ssDNA ladder (10–200 nts: ss20 DNA ladder; Simplex Sciences) was run in a parallel lane in all experiments. The gels were dried, exposed to an Imaging screen-K (Bio-Rad), and scanned using a Typhoon FLA 9500 phosphorimager (GE Healthcare). NTA reactions were done as described for TS reactions but in the absence of acceptor oligonucleotide.

PE assays

PE reactions with GsI-IIC RT were carried out by using a 50-nt and 5′-labeled DNA primer (PE primer) annealed near the 3′ end of a 1.1-kb *in vitro*–transcribed RNA. The transcript was generated by T3 runoff transcription (T3 MEGAscript kit; Thermo Fisher Scientific) of pBluescript KS (+) (Agilent) linearized using XmnI (New England Biolabs) and cleaned up using a MEGAclear kit (Thermo Fisher Scientific). The labeled DNA primer was mixed with the RNA template at a ratio of 1:1.2 and annealed by heating to 82 °C for 2 min followed by slowly cooling to room temperature to yield a final duplex concentration of 250 nM. GsI-IIC RT (200 nM) was preincubated with 20 nM of the annealed template–primer substrate in 25 μl of reaction medium containing 200 mM NaCl, 5 mM $MgCl_2$, 20 mM Tris–HCl at pH 7.5, and 5 mM DTT for 30 min at room temperature, and reverse transcription was initiated by adding 1 μl of the 25 mM dNTP mix to give a final dNTP concentration of 1 mM for each dNTP. After incubating at 60 °C for times indicated in the legends to the figures, the reaction was terminated, processed, and analyzed by electrophoresis in a denaturing 6% polyacrylamide gel, as described previously for TS reactions.

Analysis of kinetics experiments

Phosphorimager scans of reaction time courses were quantified with ImageQuant TL 8.1 (GE Healthcare) by generating rectangular boxes around the reaction products and unextended primer. For TS reactions, the quantitated products included the entire lane >2 nt longer than the labeled primer to exclude products resulting from NTA. Background was subtracted by using the same-sized rectangles on a portion of the screen that did not correspond to a gel lane. Fractions of product were plotted *versus* time and fit by a single-exponential function. For analyses of concentration dependence, rate constants were plotted against the concentration of the species being varied (RNA acceptor or dNTP in the case of NTA assays) and fit by a hyperbolic equation to obtain values of the maximal rate constant and half-maximal concentration of the varied species. Data were fitted using Prism 8 (GraphPad Software, Inc). Unless otherwise indicated, the reported uncertainty values reflect the standard error obtained from these fits.

RNA-Seq analysis of multiple template switches

TGIRT-Seq libraries were prepared as described (34, 35) by using WT and mutant F143A GsI-IIC RT using an R2 RNA–R2R starter duplex with a 1-nt 3′-DNA overhang that is composed of equimolar mix of all four nucleotides (denoted N), and a longer 24-nt acceptor RNA, whose last three nucleotides were an equimolar mix of A, C, G, and U residues (Table S1). The initial TS reactions for addition of the R2R adapter to the 5′ end of the cDNA were done as described previously with 200 nM WT or mutant GsI-IIC RT, 20 nM-unlabeled starter duplex, and 100 nM acceptor RNA for 15 min at 60 °C. After terminating the reactions with NaOH and neutralizing with HCl as described previously for TS reactions, the volume was raised to 100 μl with water, and cDNA products containing the R2R adapter attached to their 5′ end were cleaned up by using a MinElute column (Qiagen) to remove unused primer. A 5′-adenylated R1R adapter was then ligated to the 3′ end of the cDNA using Thermostable 5′ App DNA/RNA Ligase (New England Biolabs) for 1 h at 65 °C. After another MinElute clean up, the entirety of the eluent was used for a PCR with an initial 5 s denaturation step at 98 °C followed by 12 cycles of 5 s denaturation at 98 °C, 10 s annealing at 60 °C, and a 10 s extension at 72 °C using Phusion polymerase (Thermo Fisher Scientific). The resulting TGIRT-Seq libraries were then cleaned up by using 1.4× Ampure XP beads to remove residual primers, primer dimers, salts, and enzymes. The quality of the libraries was assessed by using a 2100 Bioanalyzer Instrument with a High Sensitivity DNA chip (Agilent).

The libraries were sequenced on an Illumina MiSeq v2 instrument to obtain 1 to 2 million 150-nt paired-end reads. Read 1 was used for analysis. Adaptor sequences were trimmed from Read 1 using cutadapt, version 2.10, and then processed by using a customized R script in which each read was searched for the template sequence 5′-GCCGCTTCAGAGAGAAATCGC (3′ NNN not included) allowing up to a 2-nt deletion or insertion, three mismatches, and a total of four changes (insertions, deletions, or mismatches). Error rate was calculated for both the complete 21-nt template sequence and for a 13-nt middle (core) sequence 5′-CTTCAGAGAGAAA to avoid errors near TS junctions, such as those because of mismatched base pairs, extra NTAs, or heterogeneity in the length of the synthesized oligonucleotides. Sequences of the three randomized nucleotides between two matched template sequences were used to calculate nucleotide frequencies, and the flanking sequence upstream of the first matched template in the read (the final cDNA in TS product) was used for NTA analysis. The scripts used for analysis (R script) and results were deposited under https://github.com/reykeryao/Alfred.

Data availability

The RNA-Seq data generated for this article were uploaded to BioProject ID: PRJNA723603. The structural data generated for this article were uploaded to the PDB with ID 7K9Y. All remaining data are contained within the article.

Supporting information—This article contains supporting information.

Acknowledgments—High-throughput sequencing was done by the Genomic Sequencing and Analysis Facility at the University of Texas at Austin. The Center for Biomedical Research Support at the University of Texas at Austin provided high-performance computing resources. Beamline 5.0.1 of the ALS, a US DOE Office of Science User Facility under contract no. DE-AC02-05CH11231, is supported in part by the ALS-ENABLE program funded by the National Institutes of Health, National Institute of General Medical Sciences, grant P30 GM124169-01.

Author contributions—A. M. Lentzsch, R. R., and A. M. L. conceptualization; A. M. Lentzsch, J. Y., and R. R. methodology; J. Y. software; A. M. Lentzsch, J. L. S., and R. R., validation; A. M. Lentzsch, J. L. S., J. Y., and R. R. formal analysis; A. M. Lentzsch and J. L. S. investigation; A. M. L. resources; A. M. Lentzsch, J. L. S., J. Y., and R. R. data curation; A. M. Lentzsch, J. L. S., R. R., and A. M. L. writing-original draft; A. M. Lentzsch, J. L. S., J. Y., R. R., and A. M. L. writing-review and editing; A. M. Lentzsch, J. L. S., and J. Y. visualization; A. M. L. supervision; A. M. L. project administration; and A. M. L. funding acquisition.

Funding and additional information—This work was supported by the National Institutes of Health grants R35 GM136216 (to A. M. Lambowitz) and R35 GM131777 (to R. R.). The content is solely the responsibility of the authors and does not necessarily represent the official views of the National Institutes of Health.

Conflict of interest—Thermostable group II intron RT enzymes and methods for their use are the subject of patents and patent applications that have been licensed by the University of Texas and East Tennessee State University to InGex, LLC. A. M. Lambowitz, some former and present members of the Lambowitz laboratory, and the University of Texas are minority equity holders in InGex, LLC, and receive royalty payments from the sale of TGIRT enzymes and kits employing TGIRT TS activity and from the sublicensing of intellectual property to other companies. All other authors declare that they have no conflicts of interest with the contents of this article.

Abbreviations—The abbreviations used are: cDNA, complementary DNA; CV, column volume; LTR, long terminal repeat; NTA, non-templated nucleotide addition; NTE, N-terminal extension; PDB, Protein Data Bank; PE, primer extension; RdRP, RNA-dependent RNA polymerase; RT, reverse transcriptase; TGIRT, thermostable group II intron reverse transcriptase; TS, template switching.

References

1. Coffin, J. M. (1979) Structure, replication, and recombination of retrovirus genomes: Some unifying hypotheses. *J. Gen. Virol.* **42**, 1–26
2. Lambowitz, A. M., and Belfort, M. (2015) Mobile bacterial group II introns at the Crux of eukaryotic evolution. *Microbiol. Spectr.* **3**. MDNA3-0050-2014
3. Shih, C., Yang, C. C., Choijilsuren, G., Chang, C. H., and Liou, A. T. (2018) Hepatitis B virus. *Trends Microbiol.* **26**, 386–387
4. Martin-Alonso, S., Frutos-Beltran, E., and Menendez-Arias, L. (2021) Reverse transcriptase: From transcriptomics to genome editing. *Trends Biotechnol.* **39**, 194–210
5. Inouye, S., Hsu, M. Y., Eagle, S., and Inouye, M. (1989) Reverse transcriptase associated with the biosynthesis of the branched RNA-linked msDNA in Myxococcus xanthus. *Cell* **56**, 709–717
6. Matsuura, M., Saldanha, R., Ma, H., Wank, H., Yang, J., Mohr, G., Cavanagh, S., Dunny, G. M., Belfort, M., and Lambowitz, A. M. (1997) A bacterial group II intron encoding reverse transcriptase, maturase, and DNA endonuclease activities: Biochemical demonstration of maturase activity and insertion of new genetic information within the intron. *Genes Dev.* **11**, 2910–2924
7. Kojima, K. K., and Kanehisa, M. (2008) Systematic survey for novel types of prokaryotic retroelements based on gene neighborhood and protein architecture. *Mol. Biol. Evol.* **25**, 1395–1404
8. Zimmerly, S., and Wu, L. (2015) An unexplored diversity of reverse transcriptases in bacteria. *Microbiol. Spectr.* **3**. MDNA3-0058-2014
9. Mestre, M. R., Gonzalez-Delgado, A., Gutierrez-Rus, L. I., Martinez-Abarca, F., and Toro, N. (2020) Systematic prediction of genes functionally associated with bacterial retrons and classification of the encoded tripartite systems. *Nucleic Acids Res.* **48**, 12632–12647
10. Liu, M., Deora, R., Doulatov, S. R., Gingery, M., Eiserling, F. A., Preston, A., Maskell, D. J., Simons, R. W., Cotter, P. A., Parkhill, J., and Miller, J. F. (2002) Reverse transcriptase-mediated tropism switching in Bordetella bacteriophage. *Science* **295**, 2091–2094
11. Silas, S., Mohr, G., Sidote, D. J., Markham, L. M., Sanchez-Amat, A., Bhaya, D., Lambowitz, A. M., and Fire, A. Z. (2016) Direct CRISPR spacer acquisition from RNA by a natural reverse transcriptase-Cas1 fusion protein. *Science* **351**, aad4234
12. Millman, A., Bernheim, A., Stokar-Avihail, A., Fedorenko, T., Voichek, M., Leavitt, A., Oppenheimer-Shaanan, Y., and Sorek, R. (2020) Bacterial retrons function in anti-phage defense. *Cell* **183**, 1551–1561.e1512
13. Gao, L., Altae-Tran, H., Bohning, F., Makarova, K. S., Segel, M., Schmid-Burgk, J. L., Koob, J., Wolf, Y. I., Koonin, E. V., and Zhang, F. (2020) Diverse enzymatic activities mediate antiviral immunity in prokaryotes. *Science* **369**, 1077–1084
14. Zhu, Y. Y., Machleder, E. M., Chenchik, A., Li, R., and Siebert, P. D. (2001) Reverse transcriptase template switching: A SMART approach for full-length cDNA library construction. *Biotechniques* **30**, 892–897
15. Picelli, S., Bjorklund, A. K., Faridani, O. R., Sagasser, S., Winberg, G., and Sandberg, R. (2013) Smart-seq2 for sensitive full-length transcriptome profiling in single cells. *Nat. Methods* **10**, 1096–1098
16. Wulf, M. G., Maguire, S., Humbert, P., Dai, N., Bei, Y., Nichols, N. M., Correa, I. R., Jr., and Guan, S. (2019) Non-templated addition and template switching by Moloney murine leukemia virus (MMLV)-based reverse transcriptases co-occur and compete with each other. *J. Biol. Chem.* **294**, 18220–18231
17. Golinelli, M. P., and Hughes, S. H. (2002) Nontemplated base addition by HIV-1 RT can induce nonspecific strand transfer *in vitro*. *Virology* **294**, 122–134
18. Basu, V. P., Song, M., Gao, L., Rigby, S. T., Hanson, M. N., and Bambara, R. A. (2008) Strand transfer events during HIV-1 reverse transcription. *Virus Res.* **134**, 19–38
19. Oz-Gleenberg, I., Herschhorn, A., and Hizi, A. (2011) Reverse transcriptases can clamp together nucleic acids strands with two complementary bases at their 3′-termini for initiating DNA synthesis. *Nucleic Acids Res.* **39**, 1042–1053
20. Oz-Gleenberg, I., Herzig, E., Voronin, N., and Hizi, A. (2012) Substrate variations that affect the nucleic acid clamp activity of reverse transcriptases. *FEBS J.* **279**, 1894–1903
21. Xiong, Y., and Eickbush, T. H. (1990) Origin and evolution of retroelements based upon their reverse transcriptase sequences. *EMBO J.* **9**, 3353–3362

22. Blocker, F. J., Mohr, G., Conlan, L. H., Qi, L., Belfort, M., and Lambowitz, A. M. (2005) Domain structure and three-dimensional model of a group II intron-encoded reverse transcriptase. *RNA* **11**, 14–28
23. Mohr, S., Ghanem, E., Smith, W., Sheeter, D., Qin, Y., King, O., Polioudakis, D., Iyer, V. R., Hunicke-Smith, S., Swamy, S., Kuersten, S., and Lambowitz, A. M. (2013) Thermostable group II intron reverse transcriptase fusion proteins and their use in cDNA synthesis and next-generation RNA sequencing. *RNA* **19**, 958–970
24. Stamos, J. L., Lentzsch, A. M., and Lambowitz, A. M. (2017) Structure of a thermostable group II intron reverse transcriptase with template-primer and its functional and evolutionary implications. *Mol. Cell* **68**, 926–939.e924
25. Onafuwa-Nuga, A., and Telesnitsky, A. (2009) The remarkable frequency of human immunodeficiency virus type 1 genetic recombination. *Microbiol. Mol. Biol. Rev.* **73**, 451–480
26. Hu, W. S., and Hughes, S. H. (2012) HIV-1 reverse transcription. *Cold Spring Harb. Perspect. Med.* **2**, a006882
27. Lentzsch, A. M., Yao, J., Russell, R., and Lambowitz, A. M. (2019) Template-switching mechanism of a group II intron-encoded reverse transcriptase and its implications for biological function and RNA-Seq. *J. Biol. Chem.* **294**, 19764–19784
28. Qu, G., Kaushal, P. S., Wang, J., Shigematsu, H., Piazza, C. L., Agrawal, R. K., Belfort, M., and Wang, H. W. (2016) Structure of a group II intron in complex with its reverse transcriptase. *Nat. Struct. Mol. Biol.* **23**, 549–557
29. Zhao, C., and Pyle, A. M. (2016) Crystal structures of a group II intron maturase reveal a missing link in spliceosome evolution. *Nat. Struct. Mol. Biol.* **23**, 558–565
30. Haack, D. B., Yan, X., Zhang, C., Hingey, J., Lyumkis, D., Baker, T. S., and Toor, N. (2019) Cryo-EM structures of a group II intron reverse splicing into DNA. *Cell* **178**, 612–623.e612
31. Sarafianos, S. G., Das, K., Ding, J., Boyer, P. L., Hughes, S. H., and Arnold, E. (1999) Touching the heart of HIV-1 drug resistance: The fingers close down on the dNTP at the polymerase active site. *Chem. Biol.* **6**, R137–R146
32. Johnson, K. A. (2010) The kinetic and chemical mechanism of high-fidelity DNA polymerases. *Biochim. Biophys. Acta* **1804**, 1041–1048
33. Gao, G., Orlova, M., Georgiadis, M. M., Hendrickson, W. A., and Goff, S. P. (1997) Conferring RNA polymerase activity to a DNA polymerase: A single residue in reverse transcriptase controls substrate selection. *Proc. Natl. Acad. Sci. U. S. A.* **94**, 407–411
34. Nottingham, R. M., Wu, D. C., Qin, Y., Yao, J., Hunicke-Smith, S., and Lambowitz, A. M. (2016) RNA-seq of human reference RNA samples using a thermostable group II intron reverse transcriptase. *RNA* **22**, 597–613
35. Qin, Y., Yao, J., Wu, D. C., Nottingham, R. M., Mohr, S., Hunicke-Smith, S., and Lambowitz, A. M. (2016) High-throughput sequencing of human plasma RNA by using thermostable group II intron reverse transcriptases. *RNA* **22**, 111–128
36. Xu, H., Yao, J., Wu, D. C., and Lambowitz, A. M. (2019) Improved TGIRT-seq methods for comprehensive transcriptome profiling with decreased adapter dimer formation and bias correction. *Sci. Rep.* **9**, 7953
37. Yao, J., Wu, D. C., Nottingham, R. M., and Lambowitz, A. M. (2020) Identification of protein-protected mRNA fragments and structured excised intron RNAs in human plasma by TGIRT-seq peak calling. *Elife* **9**, e60743
38. Boivin, V., Deschamps-Francoeur, G., Couture, S., Nottingham, R. M., Bouchard-Bourelle, P., Lambowitz, A. M., Scott, M. S., and Abou-Elela, S. (2018) Simultaneous sequencing of coding and noncoding RNA reveals a human transcriptome dominated by a small number of highly expressed noncoding genes. *RNA* **24**, 950–965
39. Das, K., Martinez, S. E., Bandwar, R. P., and Arnold, E. (2014) Structures of HIV-1 RT-RNA/DNA ternary complexes with dATP and nevirapine reveal conformational flexibility of RNA/DNA: Insights into requirements for RNase H cleavage. *Nucleic Acids Res.* **42**, 8125–8137
40. Nowak, E., Miller, J. T., Bona, M. K., Studnicka, J., Szczepanowski, R. H., Jurkowski, J., Le Grice, S. F., and Nowotny, M. (2014) Ty3 reverse transcriptase complexed with an RNA-DNA hybrid shows structural and functional asymmetry. *Nat. Struct. Mol. Biol.* **21**, 389–396
41. Zhao, C., Liu, F., and Pyle, A. M. (2018) An ultraprocessive, accurate reverse transcriptase encoded by a metazoan group II intron. *RNA* **24**, 183–195
42. Stamos, J. L., Lentzsch, A. M., Park, S. K., Mohr, G., and Lambowitz, A. M. (2020) *Non-LTR-retroelement reverse transcriptase and uses thereof.* PCT/US2018/05414. United States Patent Application Publication US 2020/0255810 A1, United States Patent Office.
43. Jamburuthugoda, V. K., and Eickbush, T. H. (2014) Identification of RNA binding motifs in the R2 retrotransposon-encoded reverse transcriptase. *Nucleic Acids Res.* **42**, 8405–8415
44. Bibillo, A., and Eickbush, T. H. (2002) The reverse transcriptase of the R2 non-LTR retrotransposon: Continuous synthesis of cDNA on non-continuous RNA templates. *J. Mol. Biol.* **316**, 459–473
45. Bibillo, A., and Eickbush, T. H. (2004) End-to-end template jumping by the reverse transcriptase encoded by the R2 retrotransposon. *J. Biol. Chem.* **279**, 14945–14953
46. Kuiper, M. T., and Lambowitz, A. M. (1988) A novel reverse transcriptase activity associated with mitochondrial plasmids of Neurospora. *Cell* **55**, 693–704
47. Chen, B., and Lambowitz, A. M. (1997) De novo and DNA primer-mediated initiation of cDNA synthesis by the mauriceville retroplasmid reverse transcriptase involve recognition of a 3' CCA sequence. *J. Mol. Biol.* **271**, 311–332
48. Baidyaroy, D., Hausner, G., and Bertrand, H. (2012) *In vivo* conformation and replication intermediates of circular mitochondrial plasmids in Neurospora and Cryphonectria parasitica. *Fungal Biol.* **116**, 919–931
49. Akins, R. A., Kelley, R. L., and Lambowitz, A. M. (1986) Mitochondrial plasmids of Neurospora: Integration into mitochondrial DNA and evidence for reverse transcription in mitochondria. *Cell* **47**, 505–516
50. Lai, M. M. (1992) RNA recombination in animal and plant viruses. *Microbiol. Rev.* **56**, 61–79
51. Cheng, C. P., and Nagy, P. D. (2003) Mechanism of RNA recombination in carmo- and tombusviruses: Evidence for template switching by the RNA-dependent RNA polymerase *in vitro*. *J. Virol.* **77**, 12033–12047
52. Cheng, C. P., Panavas, T., Luo, G., and Nagy, P. D. (2005) Heterologous RNA replication enhancer stimulates *in vitro* RNA synthesis and template-switching by the carmovirus, but not by the tombusvirus, RNA-dependent RNA polymerase: Implication for modular evolution of RNA viruses. *Virology* **341**, 107–121
53. Arnold, J. J., and Cameron, C. E. (1999) Poliovirus RNA-dependent RNA polymerase (3Dpol) is sufficient for template switching *in vitro*. *J. Biol. Chem.* **274**, 2706–2716
54. Ranjith-Kumar, C. T., Sarisky, R. T., Gutshall, L., Thomson, M., and Kao, C. C. (2004) De novo initiation pocket mutations have multiple effects on hepatitis C virus RNA-dependent RNA polymerase activities. *J. Virol.* **78**, 12207–12217
55. Wang, D., Jiang, A., Feng, J., Li, G., Guo, D., Sajid, M., Wu, K., Zhang, Q., Ponty, Y., Will, S., Liu, F., Yu, X., Li, S., Liu, Q., Yang, X. L., *et al.* (2021) The SARS-CoV-2 subgenome landscape and its novel regulatory features. *Mol. Cell* **81**, 1–13
56. Appleby, T. C., Perry, J. K., Murakami, E., Barauskas, O., Feng, J., Cho, A., Fox, D., 3rd, Wetmore, D. R., McGrath, M. E., Ray, A. S., Sofia, M. J., Swaminathan, S., and Edwards, T. E. (2015) Structural basis for RNA replication by the hepatitis C virus polymerase. *Science* **347**, 771–775
57. Wang, Q., Wu, J., Wang, H., Gao, Y., Liu, Q., Mu, A., Ji, W., Yan, L., Zhu, Y., Zhu, C., Fang, X., Yang, X., Huang, Y., Gao, H., Liu, F., *et al.* (2020) Structural basis for RNA replication by the SARS-CoV-2 polymerase. *Cell* **182**, 417–428.e413
58. Ferrer-Orta, C., Arias, A., Perez-Luque, R., Escarmis, C., Domingo, E., and Verdaguer, N. (2007) Sequential structures provide insights into the fidelity of RNA replication. *Proc. Natl. Acad. Sci. U. S. A.* **104**, 9463–9468
59. Shaik, M. M., Bhattacharjee, N., Feliks, M., Ng, K. K., and Field, M. J. (2017) Norovirus RNA-dependent RNA polymerase: A computational study of metal-binding preferences. *Proteins* **85**, 1435–1445
60. Choi, K. H., Groarke, J. M., Young, D. C., Kuhn, R. J., Smith, J. L., Pevear, D. C., and Rossmann, M. G. (2004) The structure of the RNA-

dependent RNA polymerase from bovine viral diarrhea virus establishes the role of GTP in de novo initiation. *Proc. Natl. Acad. Sci. U. S. A.* **101**, 4425–4430

61. Wu, J., Liu, W., and Gong, P. (2015) A structural overview of RNA-dependent RNA polymerases from the flaviviridae family. *Int. J. Mol. Sci.* **16**, 12943–12957

62. Ferrero, D., Ferrer-Orta, C., and Verdaguer, N. (2018) Viral RNA-dependent RNA polymerases: A structural overview. *Subcell Biochem.* **88**, 39–71

63. Kabsch, W. (2010) Xds. *Acta Crystallogr. D Biol. Crystallogr.* **66**, 125–132

64. Evans, P. R., and Murshudov, G. N. (2013) How good are my data and what is the resolution? *Acta Crystallogr. D* **69**, 1204–1214

65. Murshudov, G. N., Skubak, P., Lebedev, A. A., Pannu, N. S., Steiner, R. A., Nicholls, R. A., Winn, M. D., Long, F., and Vagin, A. A. (2011) REFMAC5 for the refinement of macromolecular crystal structures. *Acta Crystallogr. D Biol. Crystallogr.* **67**, 355–367

66. Winn, M. D., Ballard, C. C., Cowtan, K. D., Dodson, E. J., Emsley, P., Evans, P. R., Keegan, R. M., Krissinel, E. B., Leslie, A. G., McCoy, A., McNicholas, S. J., Murshudov, G. N., Pannu, N. S., Potterton, E. A., Powell, H. R., *et al.* (2011) Overview of the CCP4 suite and current developments. *Acta Crystallogr. D Biol. Crystallogr.* **67**, 235–242

67. Emsley, P., Lohkamp, B., Scott, W. G., and Cowtan, K. (2010) Features and development of Coot. *Acta Crystallogr. D Biol. Crystallogr.* **66**, 486–501